

Particle Segregation in Dense Granular Flows

John Mark Nicholas Timm Gray

School of Mathematics and Manchester Centre for Nonlinear Dynamics, The University of Manchester, Manchester M13 9PL, United Kingdom; email: nico.gray@manchester.ac.uk

**ANNUAL
REVIEWS Further**

Click [here](#) to view this article's online features:

- Download figures as PPT slides
- Navigate linked references
- Download citations
- Explore related articles
- Search keywords

Annu. Rev. Fluid Mech. 2018. 50:407–33

First published as a Review in Advance on October 20, 2017

The *Annual Review of Fluid Mechanics* is online at fluid.annualreviews.org

<https://doi.org/10.1146/annurev-fluid-122316-045201>

Copyright © 2018 John Mark Nicholas Timm Gray. This work is licensed under a Creative Commons Attribution 4.0 International License, which permits unrestricted use, distribution, and reproduction in any medium, provided the original author and source are credited. See credit lines of images or other third-party material in this article for license information.

**Keywords**

granular flow, particle segregation, avalanches, industrial flow, fingering, levees

Abstract

Granular materials composed of particles with differing grain sizes, densities, shapes, or surface properties may experience unexpected segregation during flow. This review focuses on kinetic sieving and squeeze expulsion, whose combined effect produces the dominant gravity-driven segregation mechanism in dense sheared flows. Shallow granular avalanches that form at the surface of more complex industrial flows such as heaps, silos, and rotating drums provide ideal conditions for particles to separate, with large particles rising to the surface and small particles percolating down to the base. When this is combined with erosion and deposition, amazing patterns can form in the underlying substrate. Gravity-driven segregation and velocity shear induce differential lateral transport, which may be thought of as a secondary segregation mechanism. This allows larger particles to accumulate at flow fronts, and if they are more frictional than the fine grains, they can feedback on the bulk flow, causing flow fingering, levee formation, and longer runout of geophysical mass flows.

Granular avalanche:

a shallow gravity-driven free-surface flow of grains

Kinetic sieving:

a gravity- and shear-driven percolation process in which small particles are more likely than large grains to fall down into gaps that open up beneath them

Squeeze expulsion:

the process by which particles are squeezed upwards out of a layer during shear

Gravity-driven segregation:

the combination of kinetic sieving and squeeze expulsion

Inverse grading:

particle-size distribution coarsens upwards (e.g., large over small)

1. INTRODUCTION

Shallow granular free-surface flows (or granular avalanches) are one of the most common particle transport mechanisms in industry and in our natural environment, as well as in our kitchens, e.g., pouring one's muesli into a bowl at breakfast! It is precisely these dense sheared granular flows that are highly efficient at segregating particles by size through the combined mechanisms of gravity-driven kinetic sieving (Middleton 1970) and squeeze expulsion (Savage & Lun 1988). The combination shall be termed gravity-driven segregation. There are at least ten other mechanisms for the segregation of dissimilar grains in granular flows (McCarthy 2009), including spontaneous percolation (Scott & Bridgwater 1975), convection (Ehrichs et al. 1995), fluidization (Schröter et al. 2006), inertia, collisional condensation (Jenkins & Yoon 2001), density, differential air drag, trajectory segregation (Schulze 2008), clustering (Mullin 2000), and ordered settling. However, gravity-driven segregation is the most important one, and this review focuses exclusively on it and its immediate consequences.

As particles are sheared downslope, the avalanche acts as a random fluctuating sieve in which small particles are statistically more likely than the large grains to percolate down under the action of gravity because they are more likely to fit into gaps that open up beneath them (Middleton 1970, Savage & Lun 1988). In dense frictional flows, this kinetic sieving mechanism is opposed by squeeze expulsion, which gives an equal probability for all particles to be levered upwards, resulting in a net flux of small particles to the base and large grains to the surface of the flow (Savage & Lun 1988). Once the grains have segregated vertically into inversely graded layers (with large particles above fine ones), velocity shear through the depth leads to the preferential transport of large particles toward the front, where they can be overrun, reseggregated, recirculated, and accumulated. Counterintuitively then, gravity-driven segregation leads to secondary lateral segregation, which may combine with frictional or shape differences between the particles to produce a strong feedback on the bulk flow (Pouliquen et al. 1997, Iverson & Vallance 2001).

Avalanches frequently develop at the free surface of heaps (Williams 1968), silos (Bates 1997, Schulze 2008), and rotating tumblers (Hill et al. 2004) and strongly interact with the underlying deposit through erosion and deposition. The gravity-driven segregation in the surface avalanche can therefore be preserved in the underlying deposit, often creating amazingly structured and beautiful patterns. In industry, these same patterns are problematic, often leading to severe handling difficulties that can degrade the quality of the final product (Johanson 1978, Bates 1997). Given that the bulk chemical, pharmaceutical, mining, agricultural, and food industries process a trillion kilograms of granular material per year in the United States alone (Shinbrot & Muzzio 1998), this problem is not to be underestimated. A fundamental understanding of how grains flow and segregate is therefore of wide-ranging industrial and environmental significance.

2. GRAVITY-DRIVEN SEGREGATION EXPERIMENTS

One of the principal reasons why particle segregation has remained somewhat mysterious is that it has been difficult to measure the evolving particle-size distribution to provide quantitative data with which to calibrate and test the models.

2.1. Gravity-Driven Chute Flow Experiments

Savage & Lun (1988) used a chute with a rough bed to study the segregation of large (1.4–1.68 mm) white beads and small (0.85–1.0 mm) black beads. Their apparatus is shown in **Figure 1a** and **Supplemental Video 1**. It featured a movable hopper and a series of splitter plates at the

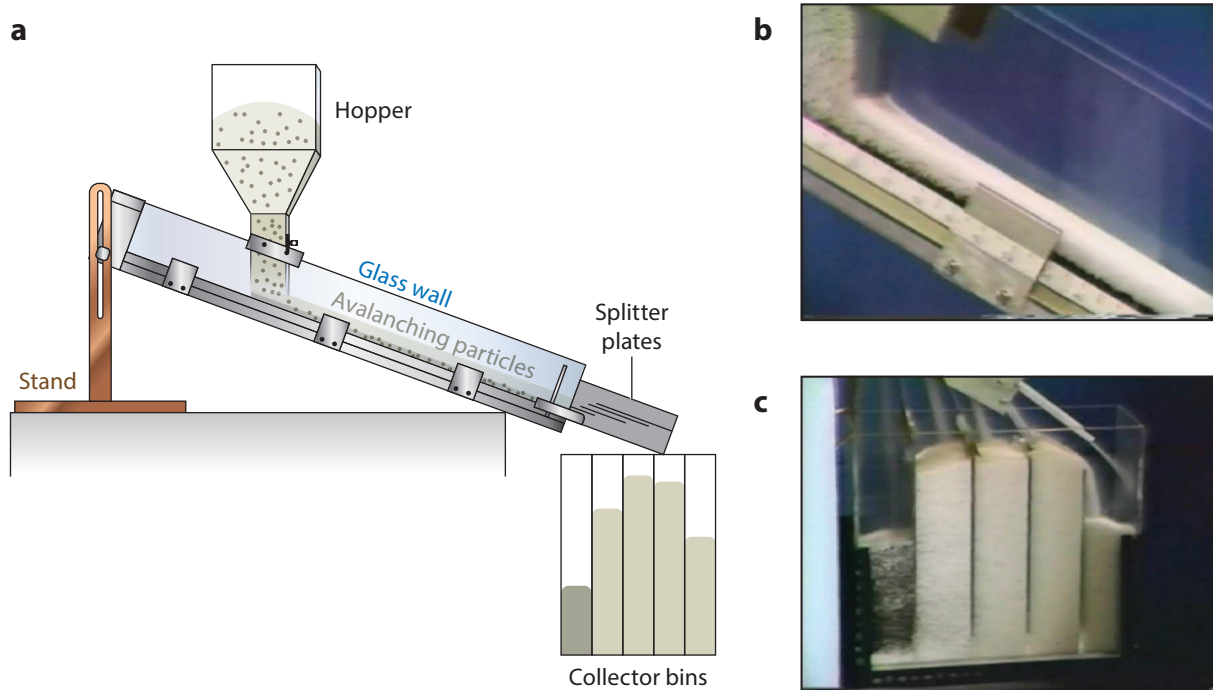


Figure 1

(a) A sketch of Savage & Lun's (1988) original chute flow experiment. Adapted with permission from Savage & Lun (1988). Photographs of (b) large (*white*) and small (*black*) particles exiting the movable hopper and flowing down the chute and (c) splitter plates separating the grains into bins at the end of the chute. Readers are also referred to **Supplemental Video 1**, courtesy of Stuart Savage.

[▶ Supplemental Material](#)

outflow that could bin up to five samples through the depth of the flow. By repeating the experiment several times with the hopper placed at different positions, they built up a series of samples of the steady-state particle-size distribution in the flowing avalanche. Savage & Lun (1988) focused on flows with relatively few small particles (10–15%) so that they could make comparisons to concentration shocks that formed in the dilute limit of their theory (see Gray & Thornton 2005 for a complete derivation). The experiments showed that for an inflow gate height of 15 mm and a slope angle of 26° , the initially well-mixed inflow separated into sharply segregated inversely graded layers, with all the large particles on top of the fine ones by 55 cm downslope (**Figure 1b,c**).

Vallance & Savage (2000) used Savage & Lun's (1988) apparatus to show that the strongest segregation occurs at angles where the material is just able to flow and that at steeper angles the particle-size distribution becomes progressively more diffuse. They also performed experiments with particles of the same size but differing density and found that the denser particles segregated to the bottom. Particle-density segregation was much weaker than particle-size segregation except at high-inclination angles, and as a result, sharp concentration shocks did not form. The rate of particle-size segregation also decreased markedly in experiments with a viscous interstitial fluid, and there was little evidence of any segregation in neutrally buoyant flows. This implies that gravity is one of the key driving mechanisms for segregation in dense sheared flows, with shear-induced segregation playing a secondary role in the absence of gravity.

Dolgunin & Ukolov (1995) and Dolgunin et al. (2006) also performed chute flow experiments. However, the best data set on steady-state segregation was obtained by Wiederseiner et al. (2011).

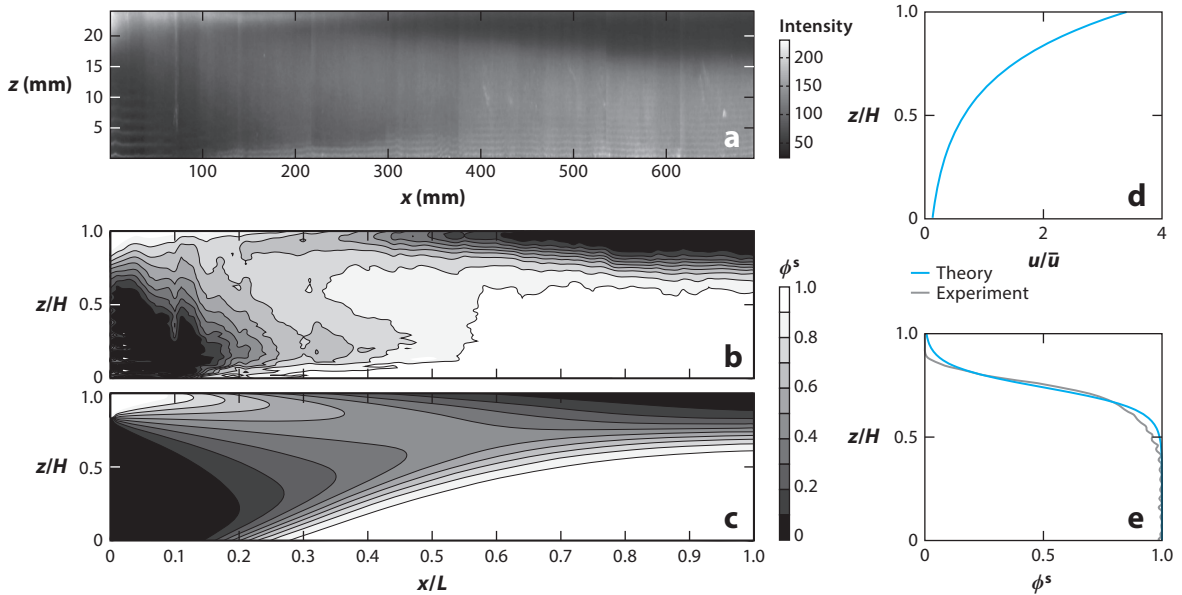


Figure 2

Experimental measurements of the steady-state small particle concentration distribution ϕ^s in a chute flow with a normally graded inflow, showing (a) a grayscale image taken through the sidewall, (b) the inferred concentration distribution $\phi^s(x, z)$, and (c) a numerical simulation using a flux-based model. The x -axis points down the chute and the z -axis is along the upward-pointing normal. The downstream velocity profile (d) is exponential with depth, and the fully developed concentration distribution (e) has an S-shaped profile. Adapted with permission from Wiedersseiner et al. (2011).

They used a high-speed camera to take 2,000 images through the transparent sidewall, averaged them in time at 10 downstream locations, and then stitched the data together to form a grayscale image of the whole chute (Figure 2a). It was then possible to use a calibration curve to infer the local concentration of small particles (Figure 2b). In an attempt to avoid three-dimensional (3D) segregation effects, they used a channel that was only 2 cm wide, which meant that the downstream velocity (Figure 2d) was affected by sidewall friction and had an exponential profile (GDR MiDi 2004). The inflow was sharply normally graded (small on top of large). As the small particles were swept downstream, they percolated down to the base of the flow, whereas the large grains rose to the surface, reaching a steady, fully developed state approximately 70 cm downstream (Figure 2a,b). The inflowing layer of small particles was much thinner than the outflowing layer due to the larger velocities, and hence larger fluxes, in the near-surface layers. Conversely, the thick layer of large particles that enters the chute becomes much thinner at the outflow. The fully developed concentration distribution (Figure 2e) is not a shock but has a smooth S-shaped inversely graded profile. This indicates that diffusive remixing due to the random collisions between the grains as they are sheared competes against gravity-driven segregation. It is possible to capture all of this behavior with relatively simple segregation models (Section 3.4).

Normal grading:

particle-size distribution coarsens downwards (e.g., small over large)

Diffusive remixing:

a diffusive effect that occurs due to the random collisions between the particles as they are sheared

2.2. Experiments in Shear Boxes and Annular Shear Cells

Some of the earliest quantitative experiments on particle-size segregation were performed by Scott & Bridgwater (1975), who used a rectangular hinged box packed with large 18.6-mm spheres that could be sheared backwards and forwards into the shape of a parallelogram. Holes were cut in the

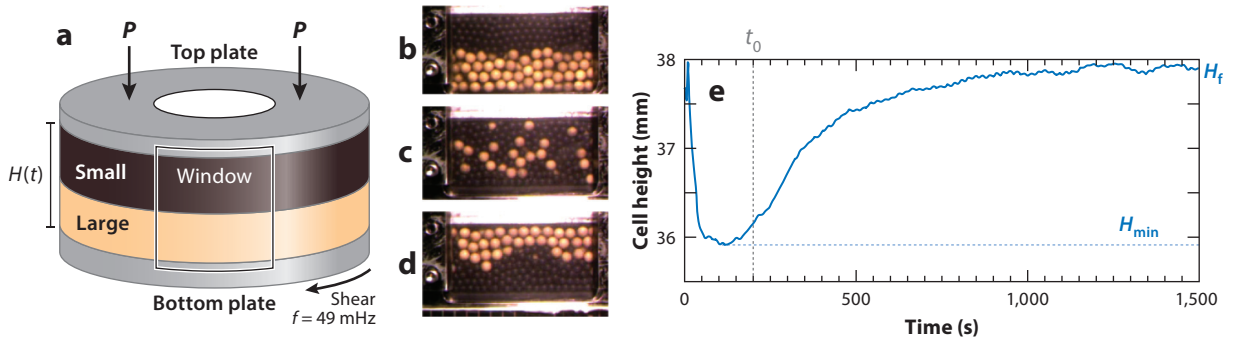


Figure 3

(a) A sketch of the annular shear cell of Golick & Daniels (2009). Photographs taken through the sidewall window show how (b) the initially sharply normally graded particles (c) mix and then (d) segregate into inversely graded layers. The height of the top plate (e) acts as a proxy for the progress of the segregation with time. Readers are also referred to **Supplemental Video 2**. Adapted with permission from Golick & Daniels (2009). Abbreviations: H_f , final top plate height; H_{\min} , minimum top plate height.

[▶ Supplemental Material](#)

base plate to allow smaller particles to be collected after percolating down from an initial position near the top of the box. Scott & Bridgwater (1975) found that by far the most important parameter controlling segregation was the grain-size ratio, with the percolation rate decreasing markedly for a grain-size ratio of 1.28 compared to 3.1.

Golick & Daniels (2009) and May et al. (2010) used an annular shear cell with a rotating bottom plate and a top plate that was free to move vertically to generate a shear flow with an exponential velocity profile (**Figure 3a**). Experiments were performed, starting from a normally graded initial state, and the evolution could be viewed through a sidewall window (**Figure 3b–d**). The particles rapidly mixed up and then resealed from one another on a much slower timescale. This correlated with the initial drop in the top plate height and its exponential recovery with time (**Figure 3e**), an effect that is due to the bidisperse mixture packing slightly more densely than either of the monodisperse phases, even during shear. Golick & Daniels (2009) found that the timescale for segregation was a nonmonotonic function of the grain-size ratio, with a peak segregation rate occurring at a grain-size ratio of two. Additionally, they found that increasing the normal pressure significantly suppressed the rate of mixing and segregation, which is indicative of the fact that dilatation of the sheared layer is important for segregation to occur. Surface avalanches, which can shear and dilate freely, therefore provide ideal conditions for segregation.

In a modern reworking of Scott & Bridgwater's (1975) experiment, van der Vaart et al. (2015) constructed a shear box with a closed base and used an index-matched fluid and a laser light sheet (**Figure 4a**) to scan across the cell after each cycle. By using information from adjacent slices, they were able to determine the size and position of every particle (**Figure 4b–d**) and hence reconstruct the temporal evolution of the small particle concentration through the depth of the cell (**Figure 4e**). These data look very similar to those obtained by Wiederseiner et al. (2011) for chute flows (**Figure 2b**), except that in this laterally uniform time-dependent problem, there are no mass flux differences with height that cause the layer thicknesses to change. The experiments were performed with a 50/50 mix of grains by volume, so all things being equal, one might expect that the first small particle would arrive at the base at the same time that the first large particle reaches the surface. The experimental data in **Figure 4e,b** show that this is not the case. Instead, there is an asymmetry that implies that a single small particle percolates rapidly down through a matrix of large grains in a series of steps, whereas a single large particle is squeezed upwards in

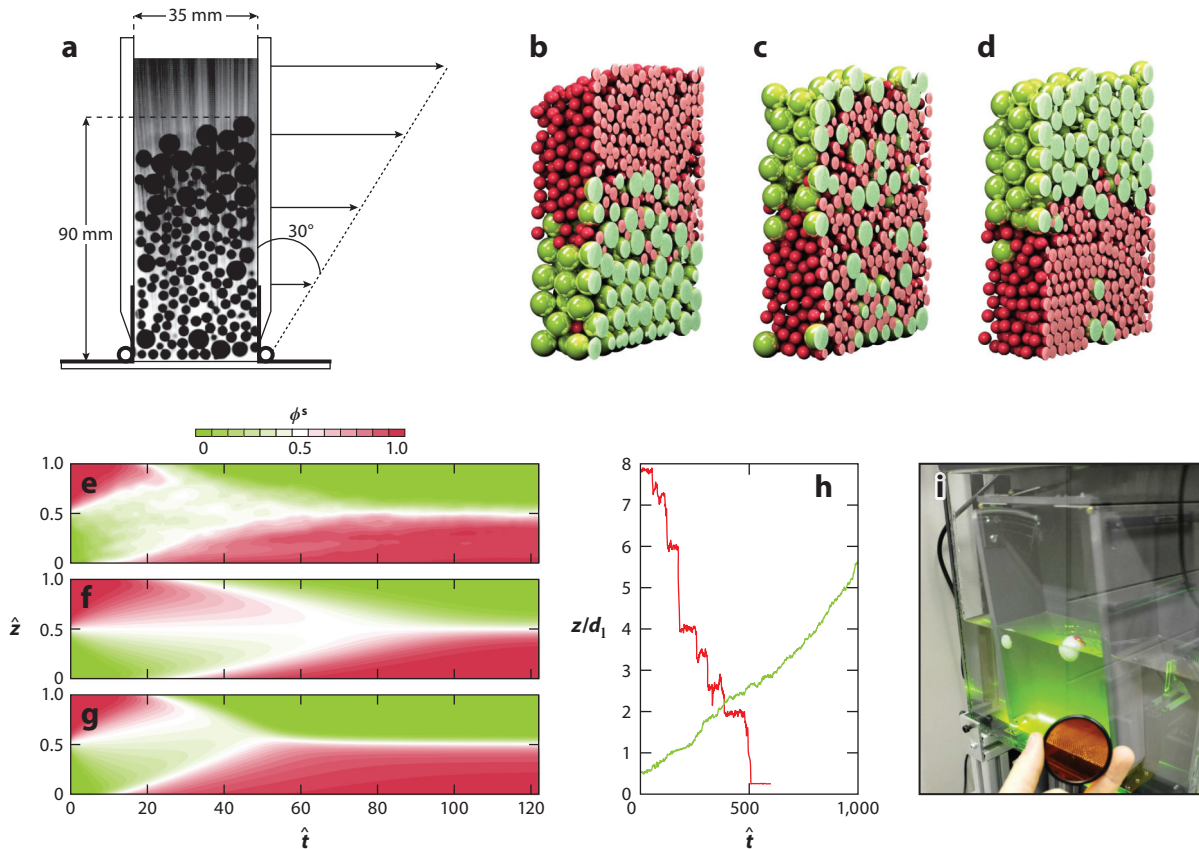


Figure 4

(a) Schematic diagram of the shear box showing the laser-illuminated plane used to (b–d) reconstruct the particle positions and (e) determine the one-dimensional evolution of the small-particle concentration in space and time. Numerical simulations of the small-particle concentration $\phi^s(z, t)$ assuming (f) a quadratic flux and (g) a cubic flux. (b) Graph of the positions of a single small (red)/large (green) particle as it percolates/rises in a matrix of large/small particles, where d_1 is the large particle diameter. Adapted with permission from van der Vaart et al. (2015). (i) Photograph of the shear box, showing a large and a medium particle in a transparent bath of small particles. Readers are referred to van der Vaart et al. (2015) for further details and to **Supplemental Videos 3 and 4**.

a slower and more continuous manner. This reflects the fact that a single large grain has many contacts with the surrounding small grains, and a collective motion is required for it to move. **Supplemental Video 3** is particularly interesting to watch, as it shows a large and a medium opaque particle rising slowly up through a matrix of transparent smaller particles (**Figure 4i**) and undergoing seemingly random rotations.

3. PARTICLE-SIZE SEGREGATION MODELS

3.1. Convective–Diffusive Structure of the Segregation Equations

The actively segregating material is often confined to a thin surface avalanche, as shown in the rotating drum experiment in **Figure 5**. An aligned coordinate system $Oxyz$ is defined with the x -axis pointing downslope at an angle ζ to the horizontal, the y -axis pointing across it, and the

Supplemental Material

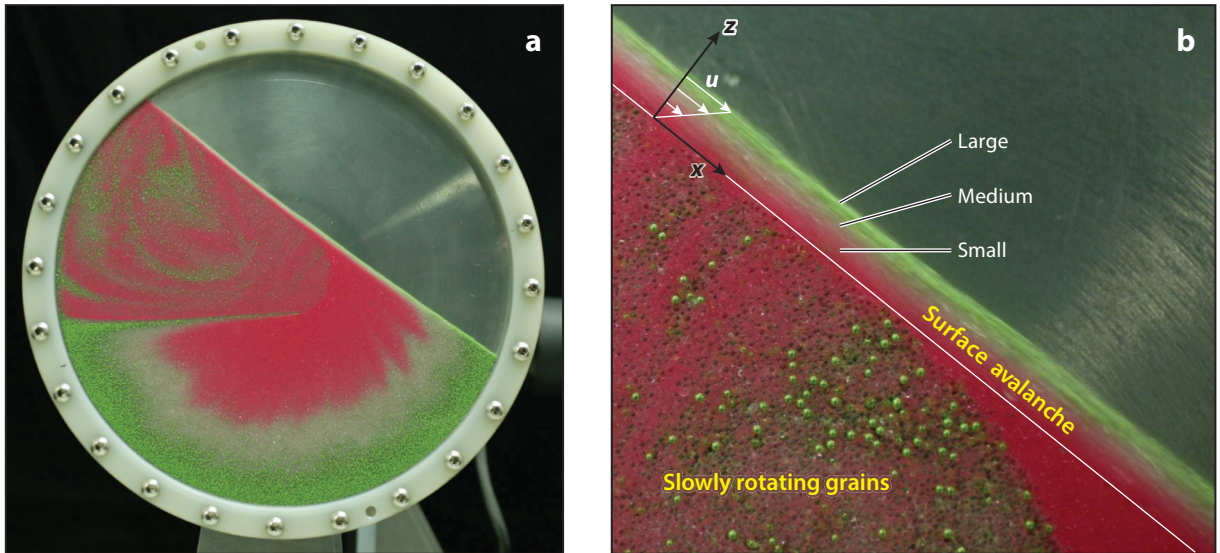


Figure 5

The formation of (a) a radial particle-size distribution in a rotating drum filled with a mixture of large green (500–750 μm), medium white (400–500 μm), and small red (75–150 μm) particles. Most of the grains are in solid-body rotation, but there is a shallow rapidly moving surface avalanche (b) where all the particle-size segregation takes place. It is useful to define a coordinate system $Oxyz$ with the x -axis pointing down the slope, the y -axis pointing across the slope and into the page and the z -axis being the upward-pointing normal. Adapted with permission from Gray & Ancy (2011).

z -axis being the upward-pointing normal. As a reasonable first approximation, the bulk velocity $\mathbf{u} = (u, v, w)$ is assumed to be incompressible,

$$\nabla \cdot \mathbf{u} = 0, \quad 1.$$

and the solids volume fraction is uniformly distributed through the avalanche depth (GDR MiDi 2004). Assuming that the mixture can be divided into a discrete distribution of grain-size classes that are relatively narrow and well-separated from one another, one can define the volume fraction $\phi^\nu \in [0, 1]$ of particles in size class ν per unit granular volume. By definition, these volume fractions sum to unity over all size classes:

$$\sum_{\nu} \phi^\nu = 1. \quad 2.$$

In the original formulation, Gray & Ancy (2011) used multicomponent mixture theory and Gray & Thornton's (2005) pressure-sharing argument to derive expressions for the percolation velocities of each species from the individual constituent momentum balances. These were then substituted into the constituent mass balances to derive a general multicomponent theory for segregation. For the purposes of illustration, it is easier to assume that each phase ν satisfies a convection–diffusion equation,

$$\frac{\partial \phi^\nu}{\partial t} + \nabla \cdot (\phi^\nu \mathbf{u}) + \nabla \cdot \mathbf{F}^\nu = \nabla \cdot (D \nabla \phi^\nu), \quad 3.$$

where \mathbf{F}^ν is the segregation flux vector for species ν , and the diffusion coefficient D is the same for all species. By summing the convection–diffusion Equation 3 over all constituents and using the summation constraint of Equation 2, one sees that the bulk velocity field \mathbf{u} is incompressible

provided that

$$\sum_v \mathbf{F}^v = \mathbf{0}. \quad 4.$$

Additionally, because percolation and squeeze expulsion (Savage & Lun 1988) are fundamentally gravity driven, the segregation flux vector is aligned with gravity, i.e.,

$$\mathbf{F}^v = -F^v \frac{\mathbf{g}}{|\mathbf{g}|}, \quad 5.$$

where $\mathbf{g} = g(\sin \zeta, 0, -\cos \zeta)$ is the gravity acceleration vector and g is the constant of gravitational acceleration. The minus sign is used to ensure that positive segregation rates correspond to particles going upwards.

Assuming the avalanche has a characteristic depth H , which is much smaller than its lateral extent L , incompressibility implies that if typical downslope velocities are of order U , then slope-normal velocities will be of magnitude εU , where the aspect ratio $\varepsilon = H/L$ is small. Typical segregation velocities are assumed to be much smaller than the downstream velocity and are also scaled as εU . This suggests the nondimensionalization

$$(x, y, z) = L(\tilde{x}, \tilde{y}, \varepsilon \tilde{z}), \quad (u, v, w) = U(\tilde{u}, \tilde{v}, \varepsilon \tilde{w}), \quad t = (L/U)\tilde{t}, \quad F^v = \frac{\varepsilon U}{\cos \zeta} \tilde{F}^v, \quad 6.$$

which, when substituted into Equation 3, implies that the component of segregation in the x -direction is of order ε and the diffusion in the x, y -plane is of order ε^2 . It follows that to leading order, the nondimensional segregation equation for constituent v is

$$\frac{\partial \phi^v}{\partial t} + \nabla \cdot (\phi^v \mathbf{u}) + \frac{\partial F^v}{\partial z} = \frac{\partial}{\partial z} \left(D_r \frac{\partial \phi^v}{\partial z} \right), \quad 7.$$

where D_r is the nondimensional coefficient of diffusive remixing and the tildes have been dropped for simplicity. The temporal evolution of the local small-particle concentration is a result of advection by the bulk flow, as well as segregation and diffusive remixing through the avalanche depth z . It should be noted that the reduced form of the segregation Equation 7 is only valid in the slope-aligned coordinate system.

3.2. Bidisperse Flux Functions and Segregation Velocities

For a bidisperse mixture, the summation constraint of Equation 2 implies that the concentration of large particles ϕ^l is equal to $1 - \phi^s$, where ϕ^s is the concentration of small grains. Additionally, Equation 4 implies $F^l = -F^s$, where the constituent letters l and s denote large and small particles, respectively. One of the most important properties of segregation models is that the small-particle flux F^s must shut off when either of the species is in a pure phase, i.e.,

$$F^s = 0 \quad \text{when} \quad \phi^s = 0, 1. \quad 8.$$

Bridgwater et al. (1985) were the first to spot this simple property and suggested purely for illustrative purposes a cubic concentration dependence,

$$F^s = -S_{ls} \phi^s (1 - \phi^s)^2 = F_{\text{Bridgwater}}, \quad 9.$$

where S_{ls} is the nondimensional segregation rate of large and small particles. Dolgunin & Ukolov (1995) suggested a quadratic function instead,

$$F^s = -S_{ls} \phi^s (1 - \phi^s) = F_{\text{Dolgunin Ukolov}}, \quad 10.$$

which has the merit that it is the simplest function that satisfies the constraints of Equation 8. Motivated by the shear box experiments of van der Vaart et al. (2015), Gajjar & Gray (2014)

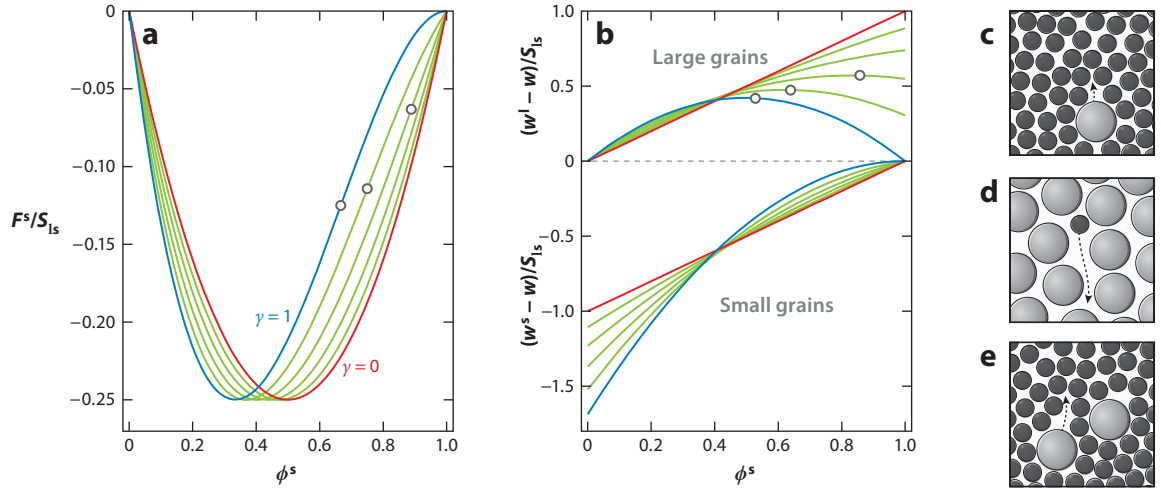


Figure 6

(a) Segregation flux functions and (b) the large- and small-particle segregation velocities for the models of Bridgwater et al. (1985) (blue), Dolgunin & Ukolov (1995) (red), and Gajjar & Gray (2014) (green), with $\gamma = 0.2, 0.4, 0.6$, and 0.8 , respectively. For $\gamma \in [1/2, 1]$, these flux functions develop an inflection point at $\phi^s_{inf} = (1 + \gamma)/(3\gamma)$ (a, white circles), and a group of large particles rises fastest at $\phi^s_{crit} = 1/(2\gamma)$ (b, white circles). (c) The slow rise of a single large particle compared to (d) the percolation of a single small grain and (e) the faster rise of a group of large particles. Adapted with permission from Gajjar & Gray (2014).

suggested the cubic segregation flux function,

$$F = -S_{ls}A_\gamma\phi(1 - \phi)(1 - \gamma\phi) = F_{\text{Gajjar Gray}}, \quad 11.$$

where the parameter $\gamma \in [0, 1]$ allows a smooth transition from the quadratic flux function of Dolgunin & Ukolov (1995) for $\gamma = 0$ to the cubic function of Bridgwater et al. (1985) for $\gamma = 1$. To make the amplitude of the flux curves comparable, one chooses the normalization factor A_γ so that the maximum magnitude of the flux is the same as for the quadratic flux function, i.e., $\max(|F^s|) = S_{ls}/4$.

The symmetric flux function of Dolgunin & Ukolov (1995) is concave everywhere, as are the asymmetric flux functions of Gajjar & Gray (2014) for $\gamma \in [0, 1/2)$ (Figure 6a). However, for $\gamma \in [1/2, 1]$, $F_{\text{Gajjar Gray}}$ develops an inflection point, which produces a zone of convexity for high small-particle concentrations. This skewing and change in convexity have a significant influence on the normal velocities of the large and small particles (Gray & Thornton 2005, Gajjar & Gray 2014), which in the absence of diffusive remixing are

$$w^1 = w - \frac{F^s(\phi^s)}{1 - \phi^s} \quad \text{and} \quad w^s = w + \frac{F^s(\phi^s)}{\phi^s}, \quad 12.$$

respectively. For the quadratic flux function of Dolgunin & Ukolov (1995), the squeeze expulsion and percolation velocities therefore have a linear dependence on concentration,

$$w^1 = w + S_{ls}\phi^s \quad \text{and} \quad w^s = w - S_{ls}(1 - \phi^s), \quad 13.$$

as shown in Figure 6b. The maximum rise rate of large particles occurs in the limit of all small particles, whereas the maximum percolation rate of fine particles occurs in the limit of all large particles (Figure 6c,d). This is also true for the cubic flux function in Equation 11, provided that $\gamma \in (0, 1/2)$. However, as γ increases, the maximum rise rate of large particles decreases, whereas

Nondimensional segregation rate of large and small particles:

$S_{ls} = qL/(HU)$, where q is a maximum segregation velocity

the maximum percolation rate of small particles progressively increases. For $\gamma \in [1/2, 1]$, the large-particle rise rate decreases so much that a group of large particles achieves maximum velocity at concentration $\phi_{\text{crit}}^s = 1/(2\gamma) \in (1/2, 1)$. Physically, this probably corresponds to a disruption to the local packing structure, so that it is easier for a group of large particles to move upwards, e.g., by reducing the number of contacts with the fine particles surrounding them (**Figure 6e**).

3.3. The Bidisperse Particle-Size Segregation Equation

Substituting the flux function in Equation 11 into Equation 7 implies that the leading order bidisperse segregation equation for the concentration of small particles $\phi^s \in [0, 1]$ is

$$\frac{\partial \phi^s}{\partial t} + \nabla \cdot (\phi^s \mathbf{u}) - \frac{\partial}{\partial z} [S_s A_\gamma \phi^s (1 - \phi^s) (1 - \gamma \phi^s)] = \frac{\partial}{\partial z} \left(D_r \frac{\partial \phi^s}{\partial z} \right), \quad 14.$$

where $\gamma \in [0, 1]$. The nondimensional segregation rate S_s and the coefficient of diffusive remixing D_r are really shorthand for functions that contain additional dependencies on other nondimensional groups such as the grain-size ratio, the solids volume fraction, and the inertial number $I = 2d \|\mathbf{D}\| / (p/\rho_s)^{1/2}$ (GDR Midi 2004), where d is the particle size, p is the pressure, ρ_s is the intrinsic density of the grains, and $\|\mathbf{D}\| = [\text{tr}(\mathbf{D}^2)/2]^{1/2}$ is a second invariant of the strain-rate tensor \mathbf{D} .

A number of authors have suggested that the segregation rate S_s is an increasing function of the strain rate (Bridgwater et al. 1985, May et al. 2010, Schlick et al. 2015). For a steady uniform Bagnold flow on an inclined plane (GDR Midi 2004), making S_s just proportional to $\|\mathbf{D}\|$ would imply that the strongest segregation occurs at the base of the flow, and the segregation rate would decay to zero at the free surface, where $\|\mathbf{D}\|$ tends to zero. However, experiments show that in Bagnold flows, particles are able to separate rapidly into almost pure layers, so a dependence of the segregation rate on inertial number seems more plausible. Even this dependence is not clear-cut, as the inertial number is a function of the monodisperse grain size d . A generalized inertial number can be defined in a bidisperse mixture by replacing the grain size d by the volume fraction-weighted average grain size, $\bar{d} = \phi^l d_l + \phi^s d_s$, where d_l and d_s are the large and small particle diameters, respectively (Rognon et al. 2007). One consequence of this is that, unlike monodisperse flows, the inertial number is no longer constant for a steady uniform flow on an inclined plane but evolves locally as the mixture segregates. Probably one of the most important consequences of the shear is that the matrix of avalanching grains dilates enough to allow particles to percolate (Golick & Daniels 2009). This is the reason why grains segregate in the surface avalanche shown in the rotating drum in **Figure 5b** but do not continue to segregate beneath it. However, once sufficient dilation has taken place for percolation to occur, one may anticipate that there is only weak dependence on shear rate or inertial number thereafter.

Mixture theory (Gray & Thornton 2005) provides a useful framework in which to derive the segregation Equation 14 and also shows that the maximum dimensional segregation velocity $q = (B/c)g \cos \zeta$ has an explicit dependence on gravity, the slope inclination ζ , and the coefficient c from the linear velocity-dependent drag law. However, the nondimensional function B , which determines how far the stresses are perturbed away from the lithostatic pressure distribution, is unknown. The functions S_s and D_r therefore have to be determined either empirically (e.g., see Savage & Lun 1988, Wiedersheimer et al. 2011, van der Vaart et al. 2015) or by discrete element model (DEM) simulations.

Coarse graining (Goldhirsch 2010, Weinhart et al. 2013) can be used to extract continuum fields from DEM simulations and hence determine useful functional laws (Rognon et al. 2007, Thornton

et al. 2012, Staron & Phillips 2014, Tunuguntla et al. 2017). This is trickier than one might expect because the segregation and the dynamics are coupled, i.e., changing the grain-size ratio or concentration changes the velocity and the frictional interaction with the base. Existing studies have therefore focused on periodic box simulations, in which the steady state is independent of the downslope velocity profile (see Section 3.4). The agreement between DEM and diffuse solutions of Equation 14 is remarkably good (Thornton et al. 2012), with the strength of the S-shaped transition determined by the Peclet number for segregation, $Pe = S_s/D_r$. Thornton et al. (2012) showed that Pe increases with increasing grain-size ratio up to a maximum at 1.7 and then decreases slightly. The most recent simulations have focused on the physical processes involved (Jing et al. 2017) and show that small particles percolate through voids without enduring contacts, whereas large particles are rolled upwards, under shear, by the frictional contacts with the surrounding particles. In particular, segregation of the large grains can be suppressed if the friction is not strong enough or if there is no rotation. DEM simulations have also been used to motivate theories that take account of kinetic stress gradients (Khakhar et al. 1999; Fan & Hill 2011; Hill & Tan 2014; Larcher & Jenkins 2013, 2015; Hill & Fan 2016) in which large particles segregate to regions of higher granular temperature.

Peclet number for segregation:
 compares the segregation velocity to the diffusion
 $Pe = S_s/D_r$

3.4. Exact and Numerical Solutions for Bidisperse Segregation

Exact solutions to the 2D bidisperse segregation Equation 14, assuming constant S_s and D_r and prescribed $b(x)$ and $\mathbf{u}(x, z)$, have greatly helped our understanding. In the inviscid case when $D_r = 0$, Equation 14 reduces to a scalar conservation law that can be solved by the method of characteristics. These reduced problems are best solved in stream function coordinates (Gray & Ancy 2009), which eliminate the explicit velocity dependence until the solutions are mapped back into physical coordinates.

Figure 7a shows the steady-state segregation from a uniformly mixed inflow (Savage & Lun 1988, Gray & Thornton 2005), which consists of three regions of constant concentration that are separated by three concentration shocks. The characteristics sweep the inflow concentration downstream unchanged, while small particles percolate downwards and large ones are squeezed upwards. At the base, however, there are no large particles to rise up; instead, the small particles separate out into a pure phase across a concentration shock whose position can be calculated using a jump condition across the discontinuity (Chadwick 1976, Gray & Thornton 2005). A similar shock develops at the surface, where a pure region of large particles forms. The two shocks eventually meet and form a third shock, which is parallel to the chute base and separates a pure region of large particles from a pure region of fine particles below. Gray et al. (2006) and Shearer et al. (2008) have constructed exact time-dependent 2D solutions to this and other cases and have shown that expanding shock regions and breaking shocks appear. Gajjar & Gray (2014) solved the steady problem with the cubic flux Equation 11 and showed for $\gamma \in [1/2, 1]$ that the lower shock may be replaced by an expansion fan or a semishock and an expansion fan, depending on the initial concentration.

When the inflow is normally graded (**Figure 7b**), the particles initially mix in an expansion fan before separating into inversely graded pure regions across three concentration shocks. The inviscid model captures the thickening and thinning of the layers observed by Wiederseiner et al. (2011) due to varying flux at different heights (**Figure 2a,b**). In **Figure 2c**, there is a numerical solution of the same problem with diffusion (Wiederseiner et al. 2011). It is very similar to the exact case except that the shocks are smoothed out. The final steady-state concentration has an

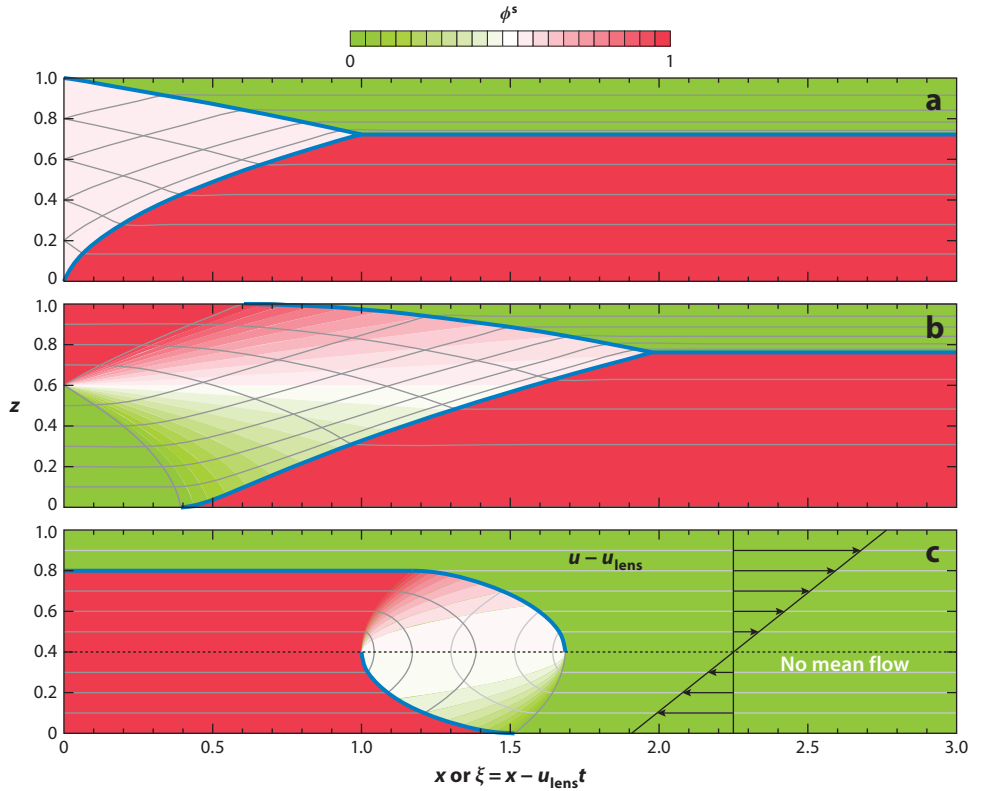


Figure 7

Two-dimensional exact solutions for (a) the steady-state small-particle concentration in a chute with a homogeneously mixed inflow (Gray & Thornton 2005), (b) the steady state for a sharply normally graded inflow (Thornton et al. 2006), and (c) a breaking size-segregation wave that travels downslope with speed $u_{\text{lens}} = 0.828$ (Thornton & Gray 2008). The segregation rate S_{Is} equals 1, D_{r} equals 0, and the downslope velocity is linear through the depth: $u = \alpha + 2(1 - \alpha)z$, with $\alpha = 1/7$. The fine gray lines show the particle paths, and the thick blue lines show the shocks.

S-shaped profile (**Figure 2e**) given by

$$\phi^s(z) = \frac{1}{1 + A \exp(\text{Pe} z)}, \quad A = \frac{\exp(-\text{Pe} \bar{\phi}) - \exp(-\text{Pe})}{1 - \exp(-\text{Pe} \bar{\phi})}, \quad \text{Pe} = \frac{S_{\text{Is}}}{D_{\text{r}}}, \quad 15.$$

where $\bar{\phi}$ is the depth-averaged concentration of small particles. Wiederseiner et al. (2011) found that typical values of the Peclet number ranged from 11 to 19 in their experiments.

Gray & Chugunov (2006) showed that 1D time-dependent problems with a quadratic flux and diffusion could be mapped to Burgers equation, and hence the Cole–Hopf transformation could be used to construct exact solutions for arbitrary initial conditions. The experiments of Golick & Daniels (2009) and van der Vaart et al. (2015) can be solved by this method. **Figure 4f** shows the grains rapidly mixing before exponentially tending toward a steady inversely graded solution, consistent with Golick & Daniels’ (2009) top-plate data. However, because the interface initially lies at $z_{\text{r}} = 1/2$, large particles reach the surface at exactly the same time that small particles reach the base, which contradicts the observation (**Figure 4e**) that small particles reach the base first.

This provides strong evidence for the cubic flux Equation 11, which is able to capture this effect (**Figure 4g**). The final steady state for the quadratic flux is given by Equation 15 with $Pe = 20.9$. Exact steady-state solutions for cubic fluxes have also been investigated by Gray & Ancey (2015).

Figure 7c shows a breaking size-segregation wave (Thornton & Gray 2008), which consists of two shocks and two expansion fans that are arranged in a lens-like structure that moves downslope with speed u_{lens} . It connects an inversely graded flow to a region of pure large particles ahead of the wave and is fundamental to the formation of large-particle-rich fronts (see Section 4). The solution is steady in a moving frame $\xi = x - u_{\text{lens}}t$. In this frame, material is swept from left to right above the no-mean-flow line and from right to left below it. Large particles that are below the no-mean-flow line are caught up by the wave and once they are overtaken by it, they rise up and eventually exit on a particle path that lies above the no-mean-flow line and move downslope faster than the wave (**Figure 7c**). Conversely, small particles that start above the no-mean-flow line catch up with the breaking wave, move down through it, and exit on a particle path that moves slower than the breaking wave. Because the wave does not occupy the full height of the flow, there is a net transport of large grains across the top, which allows the large-particle region to grow. Gajjar et al. (2016) used a gravity-driven flow on a conveyor belt to visualize the breaking wave in the moving frame using the index-matching technique (see Section 2.2). They also constructed exact solutions for the cubic flux Equation 11, which for sufficiently skewed functions allows a few large particles to take a very long time to be recirculated. Additionally, Gray & Ancey (2009) and Johnson et al. (2012) have investigated breaking waves that move at the same speed as the flow front, either by depositing the net flux of large particles that arrive at the front onto the underlying substrate or by advecting them out of plane into levees (see Section 4).

Breaking size-segregation wave:

connects inversely graded and monodisperse regions and travels steadily downslope, allowing large and small particles to be recirculated

Large-particle-rich front: a front with a high concentration of large particles

Levees: static margins that are often rich in large particles

3.5. Particle-Size and -Density Segregation and the Effect of Interstitial Fluid

The segregation Equation 14 has also been used to successfully model particle density-driven segregation (Dolgunin & Ukolov 1995; Khakhar et al. 1997, 2003; Vallance & Savage 2000; Gray & Chugunov 2006; Tripathi & Khakhar 2013; Xiao et al. 2016), and the theory has also been extended to particle-size and -density segregation (Tunuguntla et al. 2014, Gray & Ancey 2015). A cubic flux emerges naturally out of the mixture theory derivation. However, it is important to realize that the bulk velocity \mathbf{u} is no longer incompressible but satisfies the bulk mass balance,

$$\frac{\partial \rho}{\partial t} + \nabla \cdot (\rho \mathbf{u}) = 0, \quad 16.$$

where $\rho = \rho^l + \rho^s$, $\rho \mathbf{u} = \rho^l \mathbf{u}^l + \rho^s \mathbf{u}^s$, $\rho^v = \phi^v \rho^{v*}$, and ρ^{l*} and ρ^{s*} are the intrinsic densities of large and small particles, respectively (Morland 1992). The bulk density ρ therefore varies in space and time as the particles segregate. As a result, the barycentric velocity field \mathbf{u} can no longer simply be prescribed. Gray & Ancey (2015) have derived a particle-size and -density segregation equation that automatically accounts for the compressibility if the down- and cross-slope velocity components are given. Dependent on the density and grain-size ratio, a rich variety of asymmetric flux curves are generated that can be strictly positive, strictly negative, or positive and negative. Curiously, the existence of density differences between the particles makes size segregation stronger so that even small differences in particle size may compete with much larger density ratios.

A three-phase mixture theory has also been used by Thornton et al. (2006) to show that for large and small grains of intrinsic density ρ^{g*} and an interstitial fluid of density ρ^{f*} , the particle-size segregation rate is moderated by a nondimensional buoyancy term $\hat{\rho} = (\rho^{g*} - \rho^{f*})/\rho^{g*}$. If the densities of the particles and the fluid are equal, then size segregation shuts off, which is consistent with the experiments of Vallance & Savage (2000).

3.6. Flux Functions for Multiple Discrete Grain-Size Classes

In a polydisperse mixture, the segregation flux F^v of grain-size class v is closely related to the two-component case. In particular, for any two-component submixture it must reduce to precisely the bidisperse case. This suggests an additive decomposition (Gray & Ancey 2011) in which the flux of constituent v is the sum of the bidisperse flux functions with all the other phases. Given the quadratic flux model of Equation 10, this implies that

$$F^v = \sum_{\mu} S_{v\mu} \phi^v \phi^{\mu}, \quad 17.$$

where $S_{v\mu} = -S_{\mu v}$ is the nondimensional segregation rate of constituent v with respect to constituent μ . The antisymmetry property ensures that the summation constraint of Equation 4 is automatically satisfied. For a general mixture of n grain-size classes, there are n segregation equations in slope-aligned coordinates of the form

$$\frac{\partial \phi^v}{\partial t} + \nabla \cdot (\phi^v \mathbf{u}) + \frac{\partial}{\partial z} \left(\sum_{\mu} S_{v\mu} \phi^v \phi^{\mu} \right) = \frac{\partial}{\partial z} \left(D_r \frac{\partial \phi^v}{\partial z} \right). \quad 18.$$

The summation constraint of Equation 2 implies that these can be reduced to $n - 1$ independent segregation equations, which require $n(n - 1)/2$ segregation rates. In principle, these may be determined from bidisperse DEM simulations using different grain-size ratios (Thornton et al. 2012), such as those shown in **Figure 8d**.

Marks et al. (2012) have developed an alternative continuum theory for polydisperse segregation with a continuous grain-size distribution that is closer to the reality of both industrial and geophysical systems. The segregation is also driven by large particles supporting more of the stress than the fine particles (Gray & Thornton 2005), and the resulting population balance equation looks somewhat similar to the bidisperse segregation Equation 14, except that it must be solved in five dimensions: space, time, and the grain-size coordinates. Marks & Einav (2015) have also generalized cellular automata models for bidisperse segregation (Makse et al. 1997, Marks & Einav 2011) to polydisperse systems and investigated the effects of crushing and segregation, which may occur in fault gouge and pyroclastic flows.

3.7. Exact and Numerical Solutions for Polydisperse Segregation

Consider a ternary mixture of large, medium, and small particles with local concentrations ϕ^l , ϕ^m , and ϕ^s , respectively. Using the summation condition of Equation 2 to eliminate $\phi^m = 1 - \phi^s - \phi^l$, one can use the multicomponent theory of Equation 18 to yield two independent segregation equations for the concentration of large and small particles:

$$\frac{\partial \phi^l}{\partial t} + \nabla \cdot (\phi^l \mathbf{u}) + \frac{\partial}{\partial z} [S_{lm} \phi^l (1 - \phi^l - \phi^s) + S_{ls} \phi^l \phi^s] = \frac{\partial}{\partial z} \left(D_r \frac{\partial \phi^l}{\partial z} \right), \quad 19.$$

$$\frac{\partial \phi^s}{\partial t} + \nabla \cdot (\phi^s \mathbf{u}) - \frac{\partial}{\partial z} [S_{ls} \phi^s \phi^l + S_{ms} \phi^s (1 - \phi^l - \phi^s)] = \frac{\partial}{\partial z} \left(D_r \frac{\partial \phi^s}{\partial z} \right), \quad 20.$$

where S_{ls} , S_{lm} and S_{ms} are the segregation rates between the large and small, large and medium, and medium and small particles, respectively. Note that if there are no medium-sized particles, $\phi^l + \phi^s = 1$ and the system reduces to the bidisperse segregation Equation 14 with the quadratic flux function of Equation 10. In the absence of diffusion, Equations 19 and 20 form a system of hyperbolic equations, except if $S_{ls} < S_{lm}$ and $S_{ls} < S_{ms}$, when it is of mixed type for some initial concentrations, implying that it is linearly ill-posed (Joseph & Saut 1990). Such a situation is

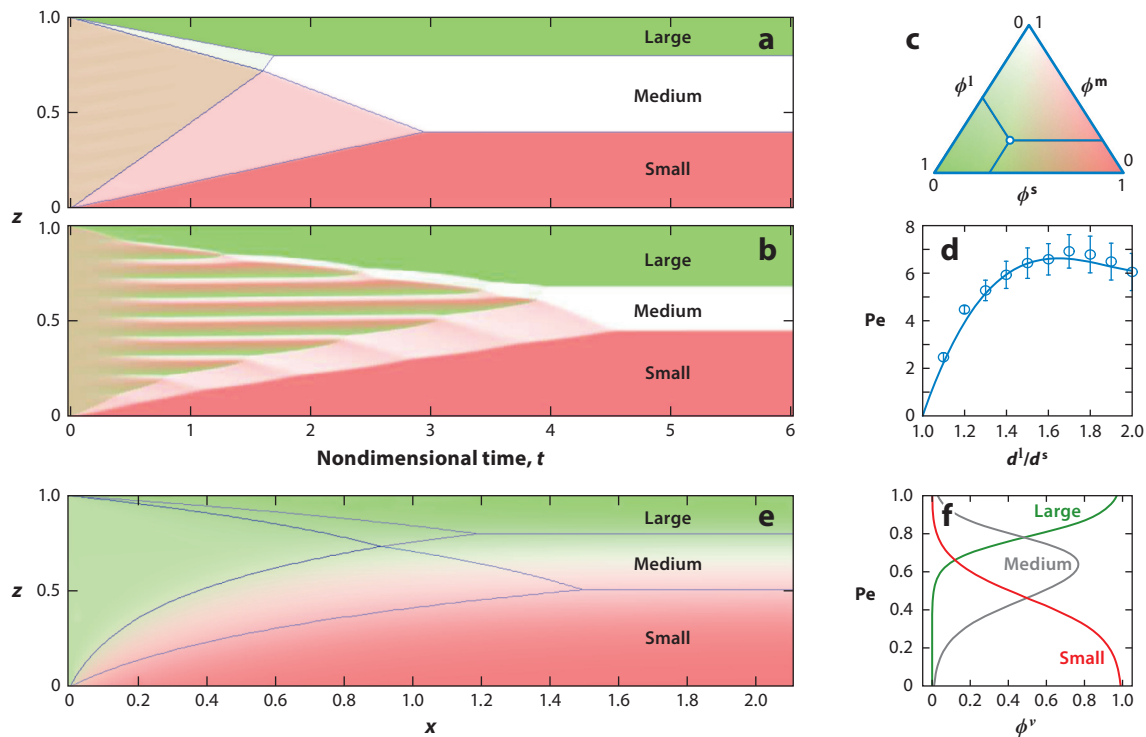


Figure 8

(*a, b*) One-dimensional (1D) time-dependent simulations of the concentration in a ternary mixture of large, medium, and small particles for $S_{ls} = 1/8$, $S_{lm} = 1$, $S_{ms} = 3/8$, and $D_r = 10^{-3}$ (Gray & Ancey 2011). The solid blue lines are the exact shock solutions in the absence of diffusion. There is a small sinusoidal perturbation to the initial concentrations of $\phi_0^l = 0.2$ and $\phi_0^s = 0.4$ (*a*) and of $\phi_0^l = 0.32$ and $\phi_0^s = 0.45$ (*b*). (*c*) The local concentration can be read off the triangular contour scale. (*d*) Discrete element model simulation of the Peclet number as a function of the grain-size ratio on a 25° slope (Thornton et al. 2012). (*e*) 2D steady-state solutions assuming an exponential downslope velocity profile $u = \beta \exp(\beta z)/[\exp(\beta) - 1]$, with $\beta = 3.3$; inflow concentrations $\phi_0^l = 1/2$ and $\phi_0^s = 1/6$; segregation rates $S_{ls} = 1$, $S_{lm} = 0.8$, and $S_{ms} = 0.5$; and $D_r = 0.05$. (*f*) Steady fully developed concentrations through the depth for the problem in panel *e* for large (*green*), medium (*gray*), and small (*red*) particles. Adapted with permission from Gray & Ancey (2011).

possible if the segregation rate $S_{v\mu}$ is a nonmonotonically increasing function of the grain-size ratio, which Golick & Daniels' (2009) experiments and Thornton et al.'s (2012) DEM simulations suggest is possible (**Figure 8d**). This provides a strong argument for the inclusion of diffusive remixing, which regularizes the system, although instabilities may still arise (Gray & Ancey 2011).

Figure 8a, b shows numerical simulations of the 1D time-dependent equations in the stable and unstable regimes, using $D_r = 10^{-3}$. The initial concentration has a small sinusoidal perturbation to an otherwise constant state that, for the unstable case, grows to form a series of stripes (**Figure 8b**), which die off as the grains segregate into two-component submixtures. An exact hyperbolic solution (Gray & Ancey 2011) consisting of six constant-concentration regions separated by eight shocks is superimposed on the stable case (**Figure 8a**). **Figure 8e** shows a steady-state 2D solution with a larger diffusion coefficient $D_r = 0.05$. The final segregated state (**Figure 8f**) has high concentrations of large particles near the surface, medium particles in the middle, and fine particles at the bottom, just like the avalanche at the surface of the rotating drum experiment shown in **Figure 5**. This is known as inverse- or reverse-distribution grading, because all the particles in the distribution are segregated into inversely graded layers by size. The strength of the

Reverse-distribution grading: the entire distribution of particles is inversely graded

Peclet number for segregation of phases ν and μ :
 $Pe^{\nu\mu} = |S_{\nu\mu}|/D_r$

Reverse coarse-tail grading: just the largest fractions of the distribution are inversely graded, and fine material is found everywhere

Granular fingering: when a uniform flow front of large rough grains and smaller less frictional particles becomes unstable

steady-state transitions is determined by the Peclet number $Pe^{\nu\mu}$ for segregation of phases ν and μ . It is stronger for large and medium particles ($Pe^{lm} = 16$) than for medium and small particles ($Pe^{ms} = 10$) in **Figure 8f**. For the exponential velocity profile used here, the shocks are shifted vertically to account for larger mass fluxes near the free surface and give a useful approximation of where to expect high concentrations of each phase at the outflow (**Figure 8e**). Gray & Ancey (2011) have also investigated solutions for reverse coarse-tail grading, where just the largest size fractions segregate into inversely graded layers, but fine particles are found throughout the mixture. Schlick et al. (2016) have also investigated polydisperse segregation in bounded heaps.

4. SECONDARY SEGREGATION DUE TO LATERAL TRANSPORT

Kinetic sieving and squeeze expulsion tend to segregate larger grains to the faster-moving free-surface layers of the flow and smaller particles toward the slower-moving base. If there is strong velocity shear, then the large and small particles may experience markedly different lateral transport. The combination of gravity-driven segregation and velocity shear can therefore be thought of as an important secondary segregation mechanism.

4.1. Segregation-Induced Levee Formation in Geophysical Mass Flows

One of the most striking examples of differential particle transport in nature occurs in debris flows (Pierson 1986, Davies 1988, Vallance & Savage 2000). Large boulders are segregated to the surface of the flow and then preferentially transported to the front by the bulk flow. Once there, they are overrun and reseggregated upward by a breaking segregation wave (**Figure 7c**), allowing the bulk flow to carry them back toward the front again (Gray & Ancey 2009). Large particles are constantly recirculated at the front, which grows in size as more and more large particles arrive from behind. Because the mobility of debris flows is intimately linked to high pore pressures (Iverson 1997, Iverson et al. 2010), large-particle-rich fronts tend to be more resistive to motion than the bulk flow, as the larger gaps between the grains allow the pore pressure to dissipate more readily. As a result, bouldery flow fronts tend to act as moving dams that hold up the more mobile material behind (Iverson & Vallance 2001).

Figure 9a shows a debris flow composed of a water-saturated mixture of sand and 32-mm rock on the 82-m-long US Geological Survey (USGS) flume (Johnson et al. 2012). Due to the strong preferential transport of large particles, the front half of the flow appears to be slightly darker than the more sandy rear half. As the flow exits the flume and flows onto the runoff pad (**Figure 9b–d**), the more resistive bouldery front wants to stop, and the coarse grains are shouldered aside by the more mobile material behind to form static lateral levees. The flow is therefore able to spontaneously form a channel, preventing the high-pore pressure, inversely graded mixture flowing down the central channel from spreading and hence allowing longer runoff. The combination of preferential large-particle transport and decreased mobility is not restricted to debris flows, but also occurs in other geophysical mass flows such as pyroclastic flows (Branney & Kokelaar 1992, Calder et al. 2000) and snow avalanches (Bartelt & Mcardell 2009).

4.2. Leveed Channels and Fingering in Small-Scale Experiments

For a continuous inflow of a bidisperse mixture of large rough grains and smaller less frictional ones, Pouliquen et al. (1997) and Pouliquen & Vallance (1999) showed that a uniform front propagating down an inclined plane broke down into a series of granular fingers (**Figure 10l**) with a lobe and cleft structure. Colored tracers were used to show that the large coarse grains

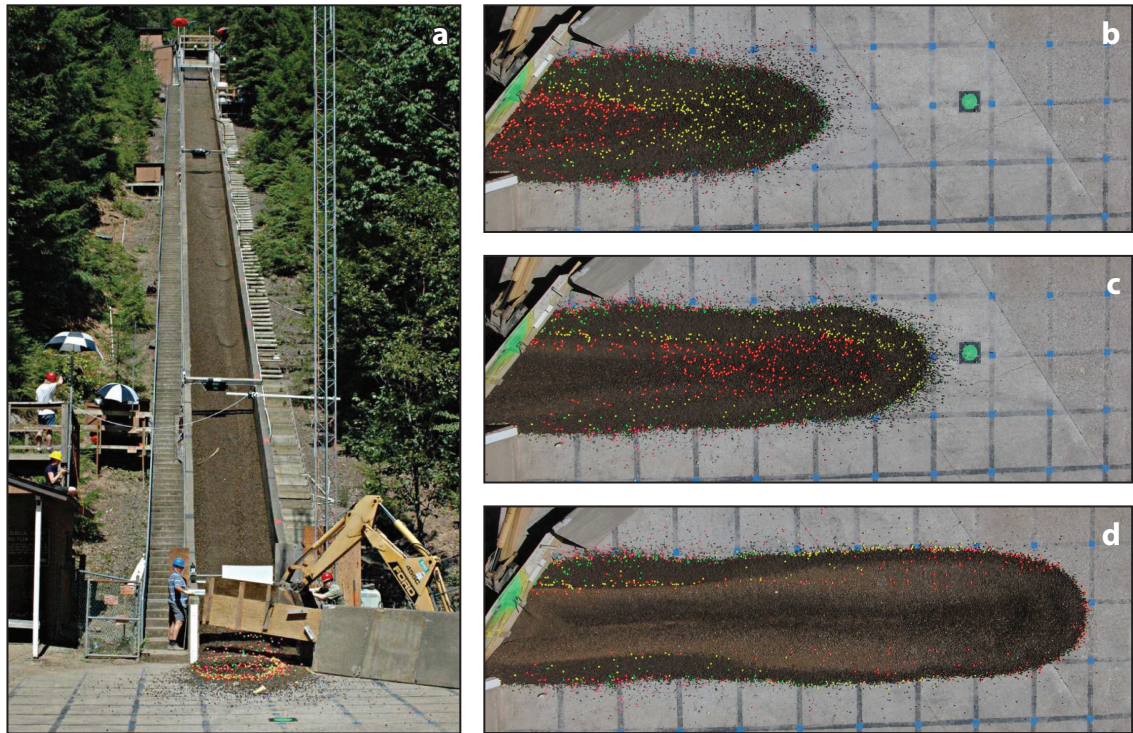


Figure 9

(a) A photograph of a debris flow, composed of sand, 32-mm rounded rock, and water, flowing down the 82-m-long US Geological Survey flume. As it emerges onto the runout pad, colored tracers are dropped on top and a sequence of overhead images (b–d) shows their motion and the formation of large rich (*darker colored*) static levees on either side of the rapidly moving (*lighter colored*) flow in the central channel. Readers are also referred to **Supplemental Videos 5–7**. Reprinted with permission from Johnson et al. (2012).

[▶ Supplemental Material](#)

were transported to the flow front and were recirculated there before being pushed into the clefts. Woodhouse et al. (2012) released a finite mass of a similar bidisperse mixture on an inclined plane, and the lobes and clefts also formed in the initial stages. However, once the supply of material to the front waned, the large-particle-rich clefts stopped, and the width of the fingers became fixed. This produced a series of discrete leveed channels that were morphologically similar to those observed at the USGS flume (**Figure 9b–d**).

Félix & Thomas (2004) showed that it was possible to generate a single leveed channel with an almost monodisperse granular material (300–400 μm), due to thinner regions being more resistive to motion than the thicker parts of the flow (Pouliquen & Forterre 2002). There were three phases of motion. Initially, the flow height increased until the channel width stabilized. Then, after a small decrease in height, there was a steady regime in which the height and width were constant and the levees were static. Finally, when the inflow ceased, the channel partially drained, leaving raised levee walls and a thinner central channel. For a bidisperse mixture of grains, Félix & Thomas (2004) found that this morphology was strongly enhanced, with the central channel almost completely drained at the end. Goujon et al. (2007) went on to show that with a bidisperse mixture of large (755 μm) and small (327 μm) beads, the runout was strongly composition dependent, with the maximum at a 40% mix of large particles.

Kokelaar et al. (2014) used an impregnation technique to capture vertical sections across the bidisperse leveed channel (**Figure 10a–e**). By changing of the color of fine particles from red to blue midway through the experiment, they showed that as the resistive coarse-grained levee was emplaced, it was also lined with fine red particles (**Figure 10d**). This provides a

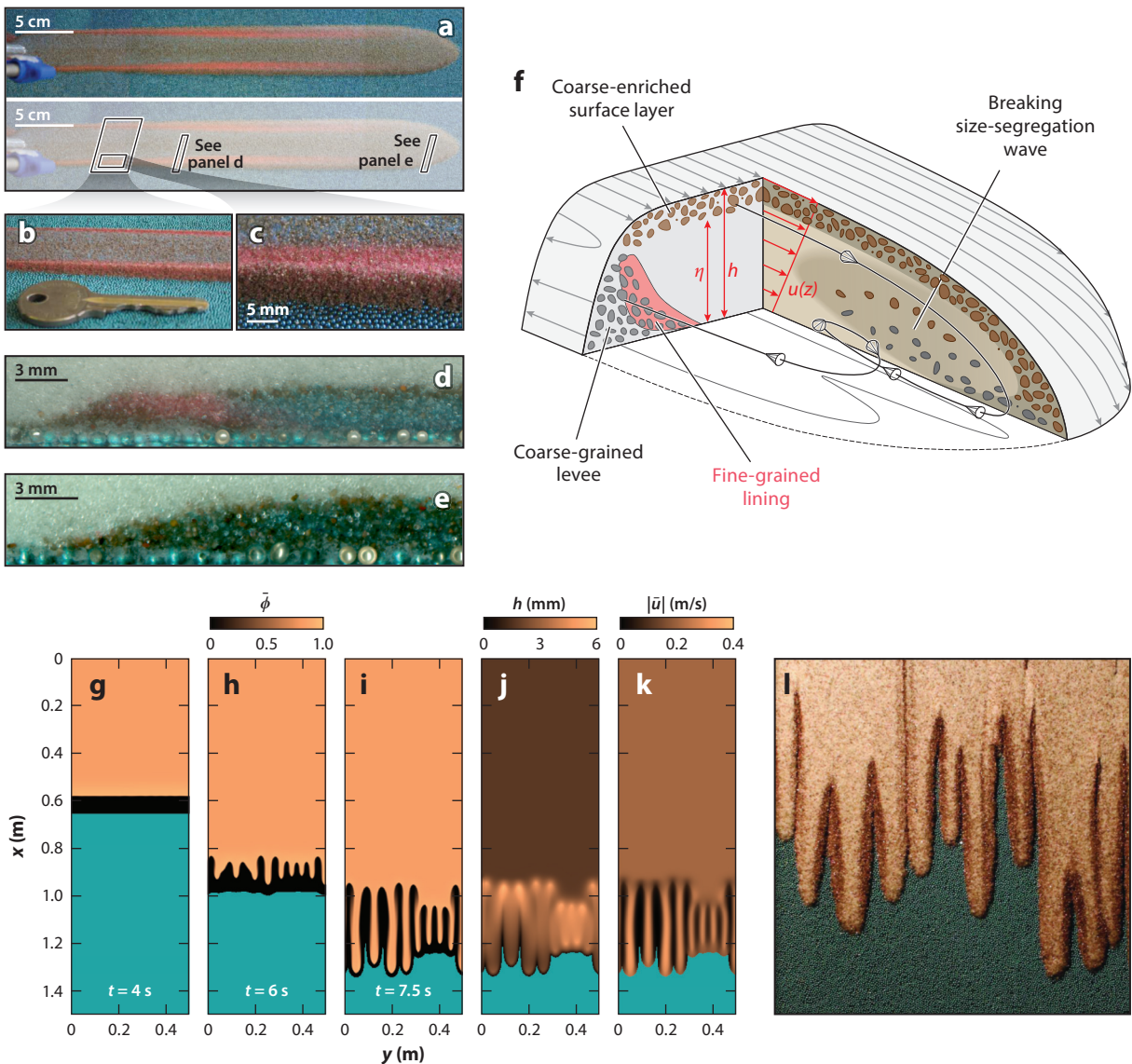


Figure 10

(a) Arrested flow of a 30/70 mix of dyed black sand (300–355 μm) and red and blue ballotini (150–250 μm) on a 29° slope. Reprinted with permission from Kokelaar et al. (2014). (b–e) Close-up views of specific locations shown in panel a. (f) Schematic diagram showing the levee-formation process. Courtesy of Chris Johnson. (g–k) Fully coupled numerical simulations of segregation-induced fingering solved using a finite-volume scheme. (l) A photograph of fingering in a bidisperse mixture of 80% white ballotini (75–150 μm) and 20% brown carborundum (305–355 μm) on a base of turquoise ballotini (750–1,000 μm). Readers are also referred to **Supplemental Videos 8 and 9**. Reprinted with permission from Baker et al. (2016b).

minimal frictional surface for the grains in the blue inversely graded central channel to flow down (**Figure 10d**). Longer runout of bidisperse leveed flows is therefore not just a result of preventing lateral spreading, but also of minimizing the basal friction. These concepts are summarized in the schematic diagram in **Figure 10f**, which shows an inversely graded central channel feeding a large-particle-rich head. Immediately behind the front is a breaking size-segregation wave that allows both large and small particles to be recirculated, forming a large-particle-rich outer levee that is lined with fine-grained material. **Figure 10e** shows a section through the breaking wave, with large particles throughout the flow depth.

Large-particle transport equation: a depth-averaged equation that segregates large particles toward the front of the avalanche and small particles toward the rear

4.3. Depth-Averaged Segregation Models

Segregation-induced levee formation is a very complicated 3D process that involves coupling between the evolving particle-size distribution and the bulk flow field. One way of simplifying the problem (Gray & Kokelaar 2010) is to use Leibniz's integral theorem to average the segregation Equation 14 through the avalanche depth b . Applying the surface and basal kinematic and no flux conditions, one obtains

$$\frac{\partial}{\partial t}(b\bar{\phi}) + \frac{\partial}{\partial x}(b\bar{\phi}u) + \frac{\partial}{\partial y}(b\bar{\phi}v) = 0, \quad 21.$$

where the depth-averaged small-particle concentration and depth-averaged small-particle fluxes in the downslope and cross-slope directions are defined as

$$\bar{\phi} = \frac{1}{b} \int_0^b \phi^s dz, \quad \bar{\phi}u = \frac{1}{b} \int_0^b \phi^s u dz, \quad \bar{\phi}v = \frac{1}{b} \int_0^b \phi^s v dz, \quad 22.$$

respectively. Explicit formulas for these integrals can be derived by making assumptions about the vertical structure through the depth of the avalanche. In particular, if the avalanche is sharply inversely graded and the velocity is linear with depth, i.e., if

$$\phi^s = \begin{cases} 0, & \eta \leq z \leq b \\ 1, & 0 \leq z \leq \eta \end{cases} \quad \text{and} \quad (u, v) = [\alpha + 2(1 - \alpha)(z/b)](\bar{u}, \bar{v}), \quad 23.$$

then

$$b\bar{\phi} = \eta, \quad \text{and} \quad (b\bar{\phi}u, b\bar{\phi}v) = \left[\eta - (1 - \alpha)\eta \left(1 - \frac{\eta}{b} \right) \right] (\bar{u}, \bar{v}), \quad 24.$$

where η is the interface height between large and small particles, the depth-averaged velocity $\bar{\mathbf{u}}$ has components (\bar{u}, \bar{v}) in the x, y -plane, and $\alpha \in [0, 1]$ allows the velocity profile to vary continuously from plug flow ($\alpha = 1$) to simple shear ($\alpha = 0$). Substituting the formulas in Equation 24 into Equation 21 and eliminating η yields the large-particle transport equation (Gray & Kokelaar 2010, Woodhouse et al. 2012, Baker et al. 2016b),

$$\frac{\partial}{\partial t}(b\bar{\phi}) + \text{div}(b\bar{\mathbf{u}}\bar{\phi}) - \text{div}[(1 - \alpha)b\bar{\mathbf{u}}\bar{\phi}(1 - \bar{\phi})] = 0, \quad 25.$$

where div is the 2D divergence operator. This equation has a term that is proportional to $\bar{\phi}(1 - \bar{\phi})$, which acts to segregate particles in a similar manner to the bidisperse segregation Equation 14 with $\gamma = 0$. The remarkable thing about this case is that small particles are segregated laterally, in the opposite direction to $\bar{\mathbf{u}}$, instead of through the avalanche depth z . Large particles are transported toward the flow front and accumulate there (hence the name). This is precisely what is required to model the USGS flume experiments (**Figure 9**) and segregation-induced levees (**Figure 10**). In this depth-averaged world, the complex structure of the breaking size-segregation waves in the full theory (**Figure 7c**) is reduced to depth-averaged concentration shocks that move at the same speed as the breaking waves (Gray & Kokelaar 2010).

4.4. Coupled Models of Segregation-Induced Fingering

The large-particle transport Equation 25 fits naturally into recent avalanche models (Gray & Edwards 2014, Baker et al. 2016a) that include depth-averaged viscous effects based on the $\mu(I)$ rheology (GDR MiDi 2004, Jop et al. 2006). The depth-averaged mass and momentum balances of such avalanche models are

$$\frac{\partial b}{\partial t} + \text{div}(b\bar{\mathbf{u}}) = 0, \quad 26.$$

$$\frac{\partial}{\partial t}(b\bar{\mathbf{u}}) + \text{div}(b\bar{\mathbf{u}} \otimes \bar{\mathbf{u}}) + \text{grad} \left(\frac{1}{2}gb^2 \cos \zeta \right) = bg\mathbf{S} + \text{div}(\nu b^{3/2}\bar{\mathbf{D}}), \quad 27.$$

where grad is the 2D gradient operator, \otimes is the dyadic product, $\bar{\mathbf{D}} = [\text{grad} \bar{\mathbf{u}} + (\text{grad} \bar{\mathbf{u}})^T]/2$ is the depth-averaged strain-rate tensor, and ν is a coefficient in the depth-averaged viscosity $\nu b^{1/2}/2$. The source term is composed of a component of gravitational acceleration that pulls the avalanche downslope and a term that resists the motion,

$$\mathbf{S} = \mathbf{i} \sin \zeta - \mu(\bar{\mathbf{u}}/|\bar{\mathbf{u}}|) \cos \zeta, \quad 28.$$

where \mathbf{i} is the unit vector in the downslope direction and μ is the effective basal friction. Pouliquen & Vallance (1999) suggested coupling the equations by assuming that μ was a depth-averaged concentration-weighted average of the large- and small-particle friction coefficients, μ^l and μ^s , i.e.,

$$\mu = \mu^l(1 - \bar{\phi}) + \mu^s\bar{\phi}, \quad 29.$$

where $\mu^l > \mu^s$ for fingering to occur. When $\nu = 0$, Equations 26 and 27 reduce to standard avalanche models (e.g., see Grigorian et al. 1967; Savage & Hutter 1989; Gray et al. 1999, 2003). However, Woodhouse et al. (2012) showed that in this case, the coupled equations are linearly ill-posed (Joseph & Saut 1990) and the finger wavelength is grid dependent. The depth-averaged $\mu(I)$ rheology (Gray & Edwards 2014) adds the key missing physics that makes the equations well-posed for $\nu > 0$.

The fully coupled viscous system of Equations 25–29 has been solved numerically by Baker et al. (2016b). After the initial release, large particles are preferentially transported to the flow front where they accumulate across a concentration shock and form a resistive margin (**Figure 10g**). The width of this layer grows with time, progressively slowing the larger particles until they are shouldered aside by the more mobile finer-grained mixture that pushes through from behind (**Figure 10h**). The fingers coarsen and begin to elongate with time (**Figure 10i**). Each finger has a pure region of slowly moving large particles at either side of the central channel, which is filled with a mixture of grains that is moving faster than the steady, uniform inflow that feeds it (**Figure 10k**). Large particles that reach the tip are continuously pushed to the side to build the levees and hence advance the finger forward. There are also more subtle effects, such as the clefts at the back of the fingers being slowly eroded by the oncoming flow, which is also observed in experiments (**Figure 10l**). There are still open questions, however. In particular, it is still not fully clear what sets the finger wavelength, because the compositional dependence of ν on $\bar{\phi}$ is not known and the levees may need to become completely static before any coarsening stops.

5. SEGREGATION WITH EROSION AND DEPOSITION

The full complexity of particle segregation becomes apparent when there is mass exchange between the free-surface avalanche, where all the gravity-driven segregation takes place, and an underlying substrate that can preserve the particle-size distribution in the deposit.

5.1. Segregation in Rotating Drums

Due to their industrial significance, there is a huge literature on segregation in rotating drums (e.g., see Khakhar et al. 1997, Hill et al. 1999, Ottino & Khakhar 2000). **Figure 5** shows a rotating drum filled with a mixture of three grain sizes (Gray & Ancey 2011). The vast majority of grains are in solid body rotation, and there is a thin avalanche along the inclined surface. The exact interface between the avalanche and the rotating material is not sharp but decays exponentially below a certain depth (GDR MiDi 2004). Nevertheless, it is still possible to see a very clear active layer in **Figure 5b** where all the segregation takes place. The initially homogeneously mixed material is slowly rotated into the active layer along the upper half of this interface (**Figure 5a**), and along the lower half, material is continuously deposited in a sequence of radial bands that coarsen toward the outside of the drum. This pattern develops because the inversely graded surface avalanche is progressively deposited from the base, with the small red particles first, then the medium white grains, and finally the large particles near the drum wall. Although the avalanche only occupies a very thin surface layer, the segregation within it completely determines the radial segregation pattern in the drum (Khakhar et al. 1997).

The way in which the avalanche flows and the way it deposits have a radical influence on the patterns observed. **Figure 11a** shows a Catherine wheel pattern (Gray & Hutter 1997, Gray & Chugunov 2006) that forms at a slower rotation rate. Intermittent avalanches flow down the inclined slope, and a shock wave propagates upslope (Gray et al. 2003), bringing the grains rapidly to rest in a thick inversely graded slope-parallel layered stripe. As the stripes are rotated, they build up the arms of the pattern. At higher rotation rates, the same grains produce a radial pattern (**Figure 11b**). Drums with noncircular cross sections produce particularly interesting patterns (Hill et al. 1999) due to the periodic rise and fall of the free surface as well as its changes in length with time (**Figure 11c**). Mounty (2007) was able to model these patterns in the continuously eroding and depositing (rolling) regime by letting the thickness of the avalanche tend to zero and by mapping the large particles that enter the avalanche instantaneously into the deposit on the lower half of the slope, with the largest grains closest to the drum wall (**Figure 11d**). This simple kinematic approach is very effective for most fill levels, but close to 50% full, the deposited grains rotate around and reenter the avalanche at the same time. As a result, particle-size segregation can feedback on the dynamics of the avalanche over a number of cycles to create petal-like patterns (**Figure 11e,f**) that are controlled by composition-dependent waves that propagate upslope, even in the rolling regime (Khakhar et al. 2003, Zuriguel et al. 2006). If the rotation rate increases, the pattern initially destroys itself before the feedback creates a new pattern with less petals.

The segregation equations introduced in Section 3 provide the basic building blocks for modeling all of these patterns. The bidisperse or polydisperse Equations 14 and 18 can be solved over the entire domain, assuming that the segregation rates $S_{v\mu}$ and the diffusive-remixing rates D_r are zero in the slowly rotating body. Incompressibility (Equation 1) then implies that they reduce to the tracer equation $\partial\phi^v/\partial t + \mathbf{u} \cdot \nabla\phi^v = 0$, so that the particle-size distribution that is deposited from the avalanche is simply rotated. The bidisperse radial segregation pattern (**Figure 11g**) can then be computed (Schlick et al. 2015) by prescribing a velocity field based on a simple mass balance model for the bulk flow in the continuously avalanching (rolling) regime (Khakhar et al. 1997, Gray 2001). At a more fundamental level, the recent advances in our understanding of the rheology of granular materials (GDR MiDi 2004; Jop et al. 2006; Kamrin & Koval 2012; Henann & Kamrin 2013; Barker et al. 2015, 2017; Barker & Gray 2017; Heyman et al. 2017) make possible fully coupled time-dependent simulations of the bulk flow and the segregation.

Radial segregation: radial bands that coarsen outward in a rotating drum and that form during a steady continuously depositing flow

Catherine wheel pattern: formed by inversely graded stripes that are laid down at the free surface and then rotated

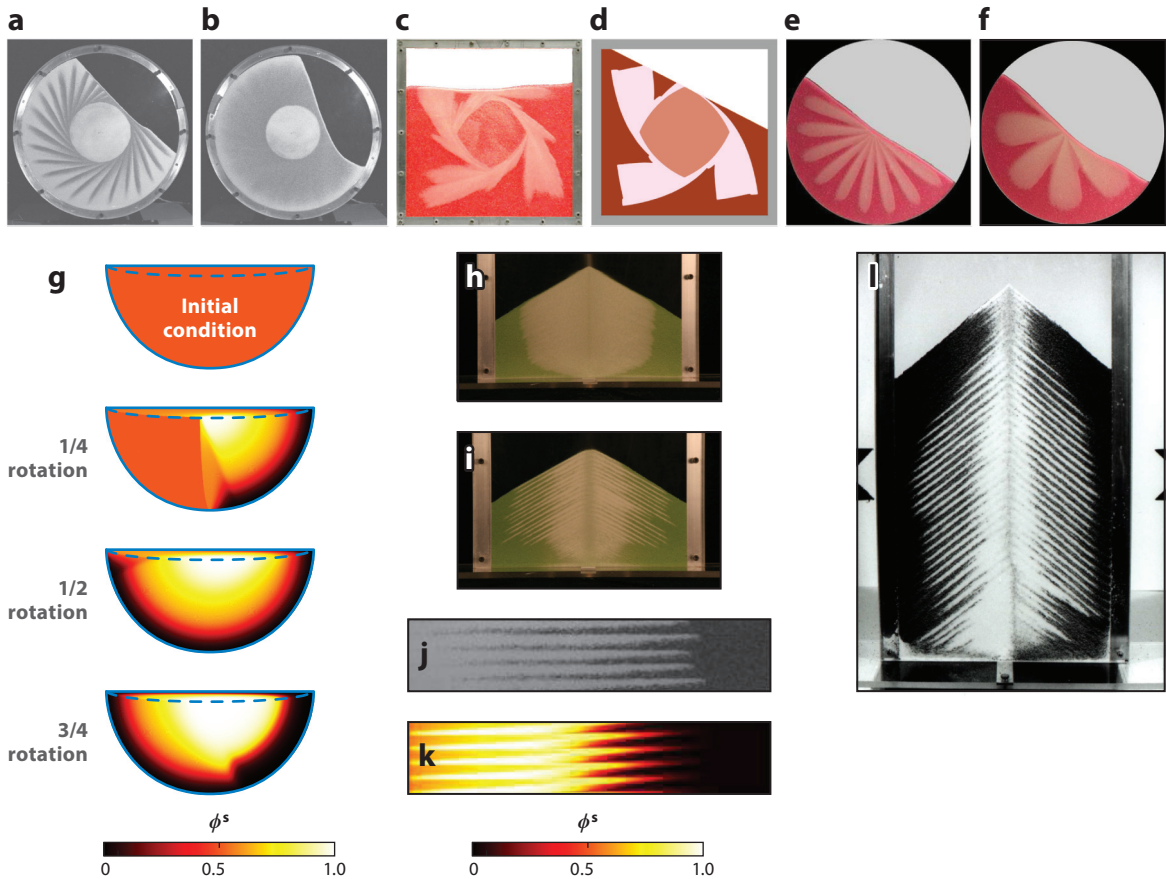


Figure 11

(a) Catherine wheel and (b) radial patterns in a bidisperse drum. Reprinted with permission from Gray & Chugunov (2006). (c,d) Continuous segregation in a square drum (Mounty 2007). (e) Petals in a 50%-full circular drum at a slower and (f) a faster rotation rate. Reprinted with permission from Zuriguel et al. (2006). (g) Simulations of radial segregation in a 50%-full drum. Adapted with permission from Schlick et al. (2015). (h) Segregated and (i) stratified heaps (Gray & Hutter 1997). (j) Rotated experiment and (k) simulation of modulated inflow on a heap (Lueptow et al. 2017). (l) Christmas tree pattern in a silo. Readers are also referred to **Supplemental Videos 10–13**. Reprinted with permission from Gray & Hutter (1998).

[▶ Supplemental Material](#)

5.2. Segregation in Heaps and Silos

Heaps and silos are the predominant means of storing granular materials and are prone to segregation due to avalanches forming at the free surface of the deposits. This is a major problem in many bulk chemical, pharmaceutical, agricultural, and food processes, especially when they are required to deliver material within narrow particle-size distributions or with specific compositions of active ingredients. The flows and deposits are closely related to those in a rotating drum. At high flow rates (Baxter et al. 1998), the surface avalanche can be in a steady state, continuously depositing the incoming grains onto the underlying substrate (**Figure 11h**), with the fine ones closest to the deposit point and the large ones closest to the base of the heap or the silo wall. This is directly analogous to radial segregation in rotating drums. At lower flow rates, the grains can build up at the apex of the pile and periodically collapse, forming intermittent avalanches that are brought to

rest by upslope propagating waves. This results in the deposit of an inversely graded stripe at the surface of the pile, which is then buried by subsequent avalanches (Gray & Hutter 1997, Gray & Tai 1998). The resulting stratification patterns (Williams 1968, Gray & Hutter 1997, Makse et al. 1997, Gray & Ancey 2009) have interleaved layers of large and small particles (**Figure 11i**) and are directly analogous to the Catherine wheel pattern in a rotating drum. Although industry would prefer their grains to be evenly mixed throughout, a stratified heap is preferable to a completely segregated one, and researchers are now investigating modulated inflows (Lueptow et al. 2017) to purposely stratify the deposit (**Figure 11j,k**). Rotational feeders, helical chargers, and other inserts are also commonly used in industry to minimize the formation of avalanches at the free surface of the deposits, where the initial segregation occurs. In addition, outflows can be drawn from different areas of the silos to try to blend the output (Bates 1997), although a fundamental understanding of how to do this effectively is still lacking. In the absence of these countermeasures, a Christmas tree pattern (**Figure 11l**) can easily form in tall silos filled from a point source.

Stratification

pattern: a deposit with alternating layers of large and small particles that are laid down by a surface avalanche

Christmas tree

pattern: forms in a silo from a point source at low flow rates and has two stratified deposits at an angle with respect to each other

SUMMARY POINTS

1. Kinetic sieving and squeeze expulsion are the dominant mechanisms for gravity-driven segregation in dense sheared granular flows that are free to dilate.
2. The combined effect can be modeled with the convection–diffusion Equation 14 in bidisperse flows and with Equation 18 in polydisperse mixtures with n size classes.
3. Velocity shear combined with gravity-driven segregation can lead to the preferential lateral transport of one species of grains. This is an important secondary segregation mechanism that can lead to the formation of bouldery margins. If large particles are more frictional than the fine particles, this can lead to dynamic feedback on the bulk flow and the formation of fingers and large-particle-rich levees.
4. Erosion and deposition between a surface avalanche, where all the segregation takes place, and an underlying substrate can produce amazingly complex patterns. This is the predominant means of segregation in rotating drums, heaps, and silos.

FUTURE ISSUES

1. The use of advanced imaging techniques and DEM simulations have the potential to revolutionize our understanding of particle segregation and tie down the functional dependencies of the nondimensional segregation and diffusive-remixing rates.
2. Progress in understanding the rheology of granular materials opens up the possibility of computing particle segregation in 3D time-dependent flows and hence of investigating mobility feedback due to differing properties of the grains.
3. The nondimensional segregation and diffusion rates are likely to be dependent on some form of generalized inertial number, which is dependent on the local concentrations and the particle sizes, rather than just a simple shear-rate dependence. Compressibility is also likely to play a very important role.
4. Particle segregation in polydisperse granular materials is a particularly open area of research that is very important for understanding real industrial and geophysical systems.

DISCLOSURE STATEMENT

The author is not aware of any biases that might be perceived as affecting the objectivity of this review.

ACKNOWLEDGMENTS

J.M.N.T.G. is very grateful for the help from colleagues in providing images for this review, which was supported by NERC grant NE/K003011/1, EPSRC grant EP/M022447/1, and Royal Society Wolfson Research Merit Award WM150058.

LITERATURE CITED

- Baker JL, Barker T, Gray JMNT. 2016a. A two-dimensional depth-averaged $\mu(I)$ -rheology for dense granular avalanches. *J. Fluid Mech.* 787:367–95
- Baker JL, Johnson CG, Gray JMNT. 2016b. Segregation-induced finger formation in granular free-surface flows. *J. Fluid Mech.* 809:168–212
- Barker T, Gray JMNT. 2017. Partial regularisation of the incompressible $\mu(I)$ -rheology for granular flow. *J. Fluid Mech.* 828:5–32
- Barker T, Schaeffer DG, Bohorquez P, Gray JMNT. 2015. Well-posed and ill-posed behaviour of the $\mu(I)$ -rheology for granular flow. *J. Fluid Mech.* 779:794–818
- Barker T, Schaeffer DG, Shearer M, Gray JMNT. 2017. Well-posed continuum equations for granular flow with compressibility and $\mu(I)$ -rheology. *Proc. R. Soc. A* 473:20160846
- Bartelt P, McArdell BW. 2009. Granulometric investigations of snow avalanches. *J. Glaciol.* 55:829–33
- Bates L. 1997. *User Guide to Segregation*, ed. GD Hayes. Marlow, UK: Br. Mater. Handl. Board
- Baxter J, Tüzün U, Heyes D, Hayati I, Fredlund P. 1998. Stratification in poured granular heaps. *Nature* 391:136
- Branney MJ, Kokelaar BP. 1992. A reappraisal of ignimbrite emplacement: progressive aggradation and changes from particulate to nonparticulate flow during emplacement of high-grade ignimbrite. *Bull. Volcanol.* 54:504–20
- Bridgwater J, Foo W, Stephens D. 1985. Particle mixing and segregation in failure zones—theory and experiment. *Powder Technol.* 41:147–58
- Calder ES, Sparks RSJ, Gardeweg MC. 2000. Erosion, transport and segregation of pumice and lithic clasts in pyroclastic flows inferred from ignimbrite at Lascar volcano, Chile. *J. Volcanol. Geotherm. Res.* 104:201–35
- Chadwick P. 1976. *Continuum Mechanics: Concise Theory and Problems*. London: Allen Unwin
- Davies TRH. 1988. *Debris flow surges: a laboratory investigation*. Tech. Rep. 96, Mitt. Versuch. Wasserbau Hydrol. Glaziologie, ETH Zurich
- Dolgunin VN, Ukolov AA. 1995. Segregation modelling of particle rapid gravity flow. *Powder Technol.* 83:95–103
- Dolgunin VN, Ukolov AA, Ivanov OO. 2006. Segregation kinetics in the rapid gravity flow of granular materials. *Theor. Found. Chem. Eng.* 40:393–404
- Ehrichs EE, Jaeger HM, Karczmar GS, Knight JB, Kuperman VY, Nagel SR. 1995. Granular convection observed by magnetic resonance imaging. *Science* 267:1632–34
- Fan Y, Hill KM. 2011. Theory for shear-induced segregation of dense granular mixtures. *New J. Phys.* 13:095009
- Félix G, Thomas N. 2004. Relation between dry granular flow regimes and morphology of deposits: formation of levées in pyroclastic deposits. *Earth Planet. Sci. Lett.* 221:197–213
- Gajjar P, Gray JMNT. 2014. Asymmetric flux models for particle-size segregation in granular avalanches. *J. Fluid Mech.* 757:297–329
- Gajjar P, van der Vaart K, Thornton AR, Johnson CG, Ancy C, Gray JMNT. 2016. Asymmetric breaking size-segregation waves in dense granular free-surface. *J. Fluid Mech.* 794:460–505
- GDR MiDi (Group. Res. Milieux Div.). 2004. On dense granular flows. *Eur. Phys. J. E* 14:341–65

- Goldhirsch I. 2010. Stress, stress asymmetry and couple stress: from discrete particles to continuous fields. *Granul. Matter* 12:239–52
- Golick LA, Daniels KE. 2009. Mixing and segregation rates in sheared granular materials. *Phys. Rev. E* 80:042301
- Goujon C, Dalloz-Dubrujeaud B, Thomas N. 2007. Bidisperse granular avalanches on inclined planes: a rich variety of behaviours. *Eur. Phys. J. E* 23:199–215
- Gray JMNT. 2001. Granular flow in partially filled slowly rotating drums. *J. Fluid Mech.* 441:1–29
- Gray JMNT, Ancey C. 2009. Segregation, recirculation and deposition of coarse particles near two-dimensional avalanche fronts. *J. Fluid Mech.* 629:387–423
- Gray JMNT, Ancey C. 2011. Multi-component particle size segregation in shallow granular avalanches. *J. Fluid Mech.* 678:535–88
- Gray JMNT, Ancey C. 2015. Particle-size and particle-density segregation in granular avalanches. *J. Fluid Mech.* 779:622–68
- Gray JMNT, Chugunov VA. 2006. Particle-size segregation and diffusive remixing in shallow granular avalanches. *J. Fluid Mech.* 569:365–98
- Gray JMNT, Edwards AN. 2014. A depth-averaged $\mu(I)$ -rheology for shallow granular free-surface flows. *J. Fluid Mech.* 755:503–34
- Gray JMNT, Hutter K. 1997. Pattern formation in granular avalanches. *Contin. Mech. Thermodyn.* 9:341–45
- Gray JMNT, Hutter K. 1998. Physik granularer Lawinen. *Phys. Bl.* 54:37–43
- Gray JMNT, Kokelaar BP. 2010. Large particle segregation, transport and accumulation in granular free-surface flows. *J. Fluid Mech.* 652:105–37. Erratum. 2010. *J. Fluid Mech.* 657:539
- Gray JMNT, Shearer M, Thornton AR. 2006. Time-dependent solutions for particle-size segregation in shallow granular avalanches. *Proc. R. Soc. A* 462:947–72
- Gray JMNT, Tai YC. 1998. Particle size segregation, granular shocks and stratification patterns. In *Physics of Dry Granular Media*, ed. HJ Herrmann, JP Hovi, S Luding, pp. 697–702. Dordrecht, Neth.: Kluwer Acad.
- Gray JMNT, Tai YC, Noelle S. 2003. Shock waves, dead-zones and particle-free regions in rapid granular free-surface flows. *J. Fluid Mech.* 491:161–81
- Gray JMNT, Thornton AR. 2005. A theory for particle size segregation in shallow granular free-surface flows. *Proc. R. Soc. A* 461:1447–73
- Gray JMNT, Wieland M, Hutter K. 1999. Free surface flow of cohesionless granular avalanches over complex basal topography. *Proc. R. Soc. A* 455:1841–74
- Grigorian SS, Eglit ME, Iakimov YL. 1967. Novaya postanovka i resheniye zadachi o dvizhenii snezhnoy laviny [A new formulation and solution of the problem of the motion of a snow avalanche]. *Tr. Vysokogorn. Geofiz. Inst.* 12:104–13
- Henann DL, Kamrin K. 2013. A predictive, size-dependent continuum model for dense granular flows. *PNAS* 110:6730–35
- Heyman J, Delannay R, Tabuteau H, Valance A. 2017. Compressibility regularizes the $\mu(I)$ -rheology for dense granular flows. *J. Fluid Mech.* 830:553–68
- Hill KM, Fan Y. 2016. Granular temperature and segregation in dense sheared particulate mixtures. *KONA Powder Part. J.* 33:150–68
- Hill KM, Gioia G, Amaravadi D. 2004. Radial segregation patterns in rotating granular mixtures: waviness selection. *Phys. Rev. Lett.* 93:224301
- Hill KM, Kharkar DV, Gilchrist JF, McCarthy JJ, Ottino JM. 1999. Segregation driven organization in chaotic granular flows. *PNAS* 96:11701–6
- Hill KM, Tan SD. 2014. Segregation in dense sheared flows: gravity, temperature gradients, and stress partitioning. *J. Fluid Mech.* 756:54–88
- Iverson RM. 1997. The physics of debris flows. *Rev. Geophys.* 35:245–96
- Iverson RM, Logan M, LaHusen RG, Berti M. 2010. The perfect debris flow? Aggregated results from 28 large-scale experiments. *J. Geophys. Res.* 115:F03005
- Iverson RM, Vallance JW. 2001. New views of granular mass flows. *Geology* 29:115–18
- Jenkins JT, Yoon D. 2001. Segregation in binary mixtures under gravity. *Phys. Rev. Lett.* 88:194301

- Jing L, Kwok CY, Leung YF. 2017. Micromechanical origin of particle size segregation. *Phys. Rev. Lett.* 118:118001
- Johanson JR. 1978. Particle segregation...and what to do about it. *Chem. Eng.* 85:183–88
- Johnson CG, Kokelaar BP, Iverson RM, Logan M, LaHusen RG, Gray JMNT. 2012. Grain-size segregation and levee formation in geophysical mass flows. *J. Geophys. Res.* 117:F01032
- Jop P, Forterre Y, Pouliquen O. 2006. A constitutive relation for dense granular flows. *Nature* 44:727–30
- Joseph DD, Saut JC. 1990. Short-wave instabilities and ill-posed initial-value problems. *Theor. Comput. Fluid Dyn.* 1:191–227
- Kamrin K, Koval G. 2012. Nonlocal constitutive relation for steady granular flow. *Phys. Rev. Lett.* 108:178301
- Khakhar DV, McCarthy JJ, Ottino JM. 1997. Radial segregation of granular mixtures in rotating cylinders. *Phys. Fluids* 9:3600–14
- Khakhar DV, McCarthy JJ, Ottino JM. 1999. Mixing and segregation of granular materials in chute flows. *Chaos* 9:594–610
- Khakhar DV, Orpe AV, Hajra SK. 2003. Segregation of granular materials in rotating cylinders. *Physica A* 318:129–36
- Kokelaar BP, Graham RL, Gray JMNT, Vallance JW. 2014. Fine-grained linings of leveed channels facilitate runoff of granular flows. *Earth Planet. Sci. Lett.* 385:172–80
- Larcher M, Jenkins JT. 2013. Segregation and mixture profiles in dense, inclined flows of two types of spheres. *Phys. Fluids* 25:113301
- Larcher M, Jenkins JT. 2015. The evolution of segregation in dense inclined flows of binary mixtures of spheres. *J. Fluid Mech.* 782:405–29
- Lueptow RM, Deng Z, Xiao H, Umbanhowar PB. 2017. Modeling segregation in modulated granular flow. *EJP Web Conf.* 140:03018
- Makse HA, Havlin S, King PR, Stanley HE. 1997. Spontaneous stratification in granular mixtures. *Nature* 386:379–82
- Marks B, Einav I. 2011. A cellular automaton for segregation during granular avalanches. *Granul. Matter* 13:211–14
- Marks B, Einav I. 2015. A mixture of crushing and segregation: the complexity of grain size in natural granular flows. *Geophys. Res. Lett.* 42:274–81
- Marks B, Rognon P, Einav I. 2012. Grain size dynamics of polydisperse granular segregation down inclined planes. *J. Fluid Mech.* 690:499–511
- May LBH, Golick LA, Phillips KC, Shearer M, Daniels KE. 2010. Shear-driven size segregation of granular materials: modeling and experiment. *Phys. Rev. E* 81:051301
- McCarthy JJ. 2009. Turning the corner in segregation. *Powder Technol.* 192:137–42
- Middleton GV. 1970. Experimental studies related to problems of flysch sedimentation. In *Flysch Sedimentology in North America*, ed. J Lajoie, pp. 253–72. Toronto: Bus. Econ. Sci. Ltd.
- Morland LW. 1992. Flow of viscous fluids through a porous deformable matrix. *Surv. Geophys.* 13:209–68
- Mounty D. 2007. *Particle size-segregation in convex rotating drums*. PhD Thesis, Univ. Manch.
- Mullin T. 2000. Coarsening of self-organised clusters in binary mixtures of particles. *Phys. Rev. Lett.* 84:4741–44
- Ottino JM, Khakhar DV. 2000. Mixing and segregation of granular materials. *Annu. Rev. Fluid Mech.* 32:55–91
- Pierson TC. 1986. Flow behavior of channelized debris flows, Mount St. Helens, Washington. In *Hillslope Processes*, ed. AD Abrahams, pp. 269–96. Boston: Allen Unwin
- Pouliquen O, Delour J, Savage SB. 1997. Fingering in granular flows. *Nature* 386:816–17
- Pouliquen O, Forterre Y. 2002. Friction law for dense granular flows: application to the motion of a mass down a rough inclined plane. *J. Fluid Mech.* 453:133–51
- Pouliquen O, Vallance JW. 1999. Segregation induced instabilities of granular fronts. *Chaos* 9:621–30
- Rognon PG, Roux JN, Naaim M, Chevoir F. 2007. Dense flows of bidisperse assemblies of disks down an inclined plane. *Phys. Fluids* 19:058101
- Savage SB, Hutter K. 1989. The motion of a finite mass of granular material down a rough incline. *J. Fluid Mech.* 199:177–215
- Savage SB, Lun CKK. 1988. Particle size segregation in inclined chute flow of dry cohesionless granular solids. *J. Fluid Mech.* 189:311–35

- Schlick CP, Fan Y, Umbanhowar PB, Ottino JM, Lueptow RM. 2015. Granular segregation in circular tumblers: theoretical model and scaling laws. *J. Fluid Mech.* 765:632–52
- Schlick CP, Isner AB, Freireich BJ, Fan Y, Umbanhowar PB, et al. 2016. A continuum approach for predicting segregation in flowing polydisperse granular materials. *J. Fluid Mech.* 797:95–109
- Schröter M, Ulrich S, Kreft J, Swift JB, Swinney HL. 2006. Mechanisms in the size segregation of a binary granular mixture. *Phys. Rev. E* 74:011307
- Schulze D. 2008. *Powders and Bulk Solids*. Berlin: Springer-Verlag
- Scott AM, Bridgwater J. 1975. Interparticle percolation: a fundamental solids mixing mechanism. *Ind. Eng. Chem. Fundam.* 14:22–27
- Shearer M, Gray JMNT, Thornton AR. 2008. Stable solutions of a scalar conservation law for particle-size segregation in dense granular avalanches. *Eur. J. Appl. Math.* 19:61–86
- Shinbrot T, Muzzio FJ. 1998. Reverse buoyancy in shaken granular beds. *Phys. Rev. Lett.* 81:4365–68
- Staron L, Phillips JC. 2014. Segregation time-scale in bi-disperse granular flows. *Phys. Fluids* 26:033302
- Thornton AR, Gray JMNT. 2008. Breaking size-segregation waves and particle recirculation in granular avalanches. *J. Fluid Mech.* 596:261–84
- Thornton AR, Gray JMNT, Hogg AJ. 2006. A three-phase mixture theory for particle size segregation in shallow granular free-surface flows. *J. Fluid Mech.* 550:1–25
- Thornton AR, Weinhart T, Luding S, Bokhove O. 2012. Modeling of particle size segregation: calibration using the discrete particle method. *Int. J. Mod. Phys. C* 23:1240014
- Tripathi A, Khakhar DV. 2013. Density difference-driven segregation in a dense granular flow. *J. Fluid Mech.* 717:643–69
- Tunuguntla DR, Bokhove O, Thornton AR. 2014. A mixture theory for size and density segregation in shallow granular free-surface flows. *J. Fluid Mech.* 749:99–112
- Tunuguntla DR, Weinhart T, Thornton AR. 2017. Comparing and contrasting size-based particle segregation models. *Comput. Part. Mech.* 4(4):387–405
- Vallance JW, Savage SB. 2000. Particle segregation in granular flows down chutes. *IUTAM Symposium on Segregation in Granular Materials*, Vol. 81, ed. AD Rosato, DL Blackmore, pp. 31–51. Dordrecht, Neth.: Springer
- van der Vaart K, Gajjar P, Epely-Chauvin G, Andreini N, Gray JMNT, Ancy C. 2015. Underlying asymmetry within particle size segregation. *Phys. Rev. Lett.* 114:238001
- Weinhart T, Hartkamp R, Thornton A, Luding S. 2013. Coarse-grained local and objective continuum description of three-dimensional granular flows down an inclined surface. *Phys. Fluids* 25:070605
- Wiederseiner S, Andreini N, Epely-Chauvin G, Moser G, Monnereau M, et al. 2011. Experimental investigation into segregating granular flows down chutes. *Phys. Fluids* 23:013301
- Williams SC. 1968. The mixing of dry powders. *Powder Technol.* 2:13–20
- Woodhouse MJ, Thornton AR, Johnson CG, Kokelaar BP, Gray JMNT. 2012. Segregation-induced fingering instabilities in granular free surface. *J. Fluid Mech.* 709:543–80
- Xiao HY, Umbanhowar PB, Ottino JM, Lueptow RM. 2016. Modelling density segregation in flowing bidisperse granular materials. *Proc. R. Soc. A* 472:20150856
- Zuriguel I, Gray JMNT, Peixinho J, Mullin T. 2006. Pattern selection by a granular wave in a rotating drum. *Phys. Rev. E* 73:061302